

Euclidean Distance Matrix Completion via Asymmetric Projected Gradient Descent

Yicheng Li , Xinghua Sun , *Member, IEEE*

Abstract—This paper proposes and analyzes a gradient-type algorithm based on Burer-Monteiro factorization, called the Asymmetric Projected Gradient Descent (APGD), for reconstructing the point set configuration from partial Euclidean distance measurements, known as the Euclidean Distance Matrix Completion (EDMC) problem. By paralleling the incoherence matrix completion framework, we show for the first time that global convergence guarantee with exact recovery of this routine can be established given $\mathcal{O}(\mu^2 r^3 \kappa^2 n \log n)$ Bernoulli random observations without any sample splitting. Unlike leveraging the tangent space Restricted Isometry Property (RIP) and local curvature of the low-rank embedding manifold in some very recent works, our proof provides new upper bounds to replace the random graph lemma under EDMC setting. The APGD works surprisingly well and numerical experiments demonstrate exact linear convergence behavior in rich-sample regions yet deteriorates fast when compared with the performance obtained by optimizing the s-stress function, i.e., the standard but unexplained non-convex approach for EDMC, if the sample size is limited. While virtually matching our theoretical prediction, this unusual phenomenon might indicate that: (i) the power of implicit regularization is weakened when specified in the APGD case; (ii) the stabilization of such new gradient direction requires substantially more samples than the information-theoretic limit would suggest.

Index Terms—Euclidean distance matrix completion, Burer-Monteiro factorization, Dual Basis.

I. INTRODUCTION

GIVEN n points $\{\mathbf{p}_i\}_{i=1}^n$ embedded in \mathbb{R}^r , $r = 2, 3$, calculating their inter-point distances is a trivial task. Forwarding the perfect, complete $n(n-1)/2$ distances back to the point set configuration is, meanwhile well-known as the classic Multi-dimensional Scaling (cMDS) [2, Sec. 3.1.1] [3] [4, Thm. 2]. However, significant efforts have been conducted to handle the case when part of the distance measurements are missing, known as the Euclidean Distance Matrix Completion (EDMC) problem [5] [4]. This not only dues to its ubiquitous presence in, e.g., computational chemistry [6] [7] [8] [9], operating wireless sensor networks [10] [11] [12] and articulated robots [5, Sec. 4.3.2] [13], channel estimation [14], indoor SLAM [15], ultrasound calibration [16], but also the fact that this inverse problem is NP-hard to solve in general [17, Sec. 3.4]. To escape from the NP-hardness, one may only consider a selected region of the ground truth (generic [18] [19], incoherence [20] [21]), enforcing certain

connectivity of the underlying sample graph (Erdős-Rényi [22] [23], random geometric graph [12] [24] [25] [26]), and posing constrains on certain geometry of the point set (r -unique localizable [27], trilateration [28], universal rigidity [29]). Therefore, performance guarantee results in this field can be roughly divided into two classes, i.e., combinatorial [27] [29] [30] and probabilistic. While the latter can be further categorized into the traditional yet effective view from random geometry [12] [24] [25] [26], and the recent revisit of EDMC via incoherent matrix completion lens [20] [23] [31] [22]. Method proposed in this manuscript belongs to the last class. In short, we analyze an algorithm analogous to the Iterative Fast Hard Thresholding for EDMC (IFHT-EDMC) that appeared in a very recent work [23], under standard incoherence assumption [32] and Bernoulli sampling scheme, from the quotient geometry perspective.

A. Related Work

We are interested in answering the following question

Q1: *Does the theoretical success of the two-step non-convex factorization type incoherent matrix completion algorithms [33] [34] [35] [36] generalize to the EDMC setting?*

While the Bernoulli sample model used in these works does not have strong real-world application scenarios when specified to EDMC, we are not aware of any work that analyzed the non-convex gradient refinement stage under a more practical sample model that depends on the magnitudes of EDM entities, i.e., the so-called unit ball rule, under the random geometry setup¹. Javanmard and Montanari developed the stability notion of a rigid graph [12, Lemma 4.1, 4.2] and use that to show the perturbation on convex solution can be bounded. [26] [24] analyzed the MAP-MDS estimator [37] by showing the shortest path algorithm faithfully returns the Euclidean distance between unconnected nodes when the point set is regular. In parallel, [25] obtained almost the same result, and they sent the surrogate produced by MAP-MDS into the OptSpace [33] for refinement. Numerically, it was demonstrated that the phase transition of OptSpace matches that of the theoretical bound on MAP-MDS. [16, Thm. 1.2] provided bounds on similar refinement step, yet they treat the EDM-dependent samples as pure additive noise and only address the Bernoulli erasures.

The original motivation for raising **Q1** comes from Tasissa and Lai [20], who showed, for the first time that a natural parallelization of the Nuclear Norm Minimization (NNM) [38] [39], called trace minimization (the trace regularized version of the Semidefinite Relaxation (SDR) of (5)), can

Part of this work [1] has been presented during the 2024 Asia Pacific Signal and Information Processing Association Annual Summit and Conference (APSIPA ASC), Macao, China. This work has been submitted to the IEEE for possible publication. Copyright may be transferred without notice, after which this version may no longer be accessible.

Y. Li and X. Sun are with the School of Electronics and Communication Engineering, Shenzhen Campus of Sun Yat-sen University, Shenzhen 518107, China (e-mail:liyich75@mail2.sysu.edu.cn; sunxinghua@mail.sysu.edu.cn).

¹We emphasize that the transition bound obtained from random geometry graph is often sharp up to constant.

solve EDMC given $\mathcal{O}(n\nu r \log^2 n)$ uniform distance samples taking at random, where ν is certain coherence parameter defined w.r.t. the EDM basis ω_α ². They also demonstrated the generalizability of this specific modification to the Golfing Scheme [40] by analyzing matrix completion problem under arbitrary set of non-orthonormal and non-sub-Gaussian basis, provided the extremal eigenvalues of the basis correlation matrix are well understand [41]. Subsequent work [42] characterized the eigen-spectrum of the correlation matrix \mathbf{H}_ω of ω_α basis, and revealed that \mathbf{H}_ω has only three types of distinct eigenvalues: $2n$, n , and 2. Such near-singular spectral structure does not significantly hinder the convergence of the Golfing Scheme, as the original inexact dual certificate requires precision on $\mathcal{O}(1/n)$ for the residual term $\|\mathcal{P}_\Omega \mathbf{Y} - \text{sgn}(\mathbf{X}^*)\|$ [32, Prop. 2], while the modified one for EDMC appears like $\mathcal{O}(\frac{\lambda_{\min}(\mathbf{H}_\omega)}{n\lambda_{\max}(\mathbf{H}_\omega)}) = \mathcal{O}(1/n^2)$ [41, Thm. 2]. Since the Golfing Scheme converges exponentially fast, the extra iteration cost for improving $1/n$ to $1/n^2$ is negligible. Yet this makes the design and analysis of non-convex methods considerably more obscure, which, in its most straightforward form, aims to solve a fourth-order polynomial as follows

$$\begin{aligned} \min_{\mathbf{P} \in \mathbb{R}^{n \times r}} h(\mathbf{P}) &:= \sum_{\alpha \in \Omega} |\langle \mathbf{P}\mathbf{P}^T, \omega_\alpha \rangle - \mathbf{D}_\alpha^*|^2, \quad (1) \\ &= \|\mathcal{P}_\Omega(g(\mathbf{P}\mathbf{P}^T) - \mathbf{D}^*)\|_F^2, \\ [\mathcal{P}_\Omega(\mathbf{D})]_{ij} &= \begin{cases} \mathbf{D}_{ij}, & \text{if } (i, j) \in \Omega \\ 0, & \text{else} \end{cases}. \end{aligned}$$

where Ω is the sample set, $\alpha = (i, j)$ is a tuple and the distance between (i, j) points, $(i, j) \in \Omega$, is known. $\mathbf{D}_\alpha^* = \langle \mathbf{D}^*, \mathbf{e}_i \mathbf{e}_j^T \rangle = \mathbf{D}_{ij}^*$ denote the sampled ground truth EDM, where \mathbf{e}_i stands for the i -th canonical Euclidean basis in \mathbb{R}^n . \mathbf{P} stands for the point set to be recovered. $\mathcal{P}_\Omega g(\cdot)$ can be viewed as the matrix wrap up of the expression $\sum_{\alpha \in \Omega} \langle \cdot, \omega_\alpha \rangle \mathbf{e}_i \mathbf{e}_j^T$ for the moment, and the precise form of g will be shortly defined below. Eq. (1) bears great resemblance to the Wirtinger Flow [43] used in phase retrieval, Hankel lift for spectral compressive sensing [44] [45], $l_{2,\infty}$ regularized free non-convex matrix completion [46] [47], and so on³. However, the large condition number of \mathbf{H}_ω prevents us from pursuing theoretical contraction speed when optimizing (1), as discussed in [22, Sec. III-C] [23, Sec. 6], even though (1) does produce an attractive basin given enough Bernoulli samples, the basin is too small when measured by $l_{2,\infty}$ norm.

Such predicament is caused by the strong diagonal dominance inherent in the ω_α basis. In short, a total sum of them gives rise to a Laplacian of a complete graph, i.e., $\mathcal{L} = n\mathbf{I} - \mathbf{1}\mathbf{1}^T$, where $\mathbf{1}$ is the vector of all ones. While one can show the sampled sum of ω_α closely approximates \mathcal{L} , controlling the distortion introduced by the $n\mathbf{I}$ term remains challenging [22, Lemma B.2]. Nevertheless, extensive numerical evidence over the years has proved that various first-order methods perform well when optimizing (1) without relying on explicit

regularization or incoherence projections. These approaches not only converge when started randomly or by simple spectral estimator under Bernoulli sample model [1], but such local search is also acknowledged to be remarkably effective in the refining stage of several SDRs [10, Sec. 5] [9, Sec. 3.2], even when the sampling model is substantially more intricate. We pause to emphasize that under Bernoulli rule, the original two-step routine, i.e., spectral initialization [49] [23, Lemma 5.6] [1, Thm. I.1] followed by Vanilla Gradient Descent (VGD) on (1), fails to match the empirical performance of trace minimization-based approaches. Such unexpected discrepancy has also been witnessed in [31, Sec. 5], where they showed the phase transition of a scaled-Stochastic Gradient Descent (SGD) [50] is evidently later than that of convex and the iterative re-weighting method.

Another interesting open question concerning (1) is the analytical justification for the observed absence of its spurious local minima, as summarized and empirically reported in [51, Ch. 3.5]. This phenomenon is particularly striking: drawing from the global landscape analysis of Zhu et al. [52, Thm. 1], one might expect that ill-conditioning of the Hessian associated with the un-factorized cost function would preclude the existence of a benign optimization landscape. Moreover, due to the lost of a smooth generalization of the random graph lemma [33, Lemma 7.1] to the EDMC settings as mentioned above, Ge et al.'s framework [53] [54], i.e., by introducing penalty term on the $l_{2,\infty}$ norm of \mathbf{P} into (1) to amend the curvature of landscape, cannot be immediately adopted. As we will elaborate further, it also remains an open question whether the standard incoherence condition adequately captures the class of EDMs that are efficiently completable in polynomial time⁴.

Given that many of these largely unexplored questions stem, at least in part, from the condition number of \mathbf{H}_ω , [23] considered using the pseudo inverse of g (denoted as g^+) to correct the condition number of the Hessian of (1). That is, to construct the following new pre-conditioned sample operator

$$\mathcal{R}_\Omega(\cdot) := g^+ \mathcal{P}_\Omega g(\cdot), \quad (2)$$

and to optimize

$$\min_{\mathbf{G} \in \mathcal{S}_+^{n,r}} F(\mathbf{G}) := \frac{1}{p} \langle \mathcal{R}_\Omega(\mathbf{G} - \mathbf{G}^*), \mathbf{G} - \mathbf{G}^* \rangle, \quad (3)$$

where $\mathcal{S}_+^{n,r}$ denotes the Positive Semidefinite (PSD) fix-rank embedding matrix manifold [55]. The major drawback is that one cannot compute $\nabla F(\mathbf{G})$ but only a part of it, which they called pseudo gradient $\hat{\nabla} F(\mathbf{G}) := \frac{2}{p} \mathcal{R}_\Omega(\mathbf{G} - \mathbf{G}^*)$. Certain trade-off arises here between maintaining self-adjointness and ensuring algorithmic explainability: since \mathbf{H}_ω^{-1} (the inverse of \mathbf{H}_ω) is not diagonal, in general we would like to evade from constructing $\mathcal{R}_\Omega^* \mathcal{R}_\Omega$ ⁵, while using \mathcal{R}_Ω alone compromises the least-squares structure. Things tend to be more subtle when one inquires about numerical performance. This Riemannian

⁴Please see [21, Thm. 4] for more discussion.

²The form of ω_α will be introduced shortly in Section II. We note that $\nu = \mathcal{O}(r\mu)$, where μ is the standard coherence parameter defined w.r.t. $\mathbf{e}_i \mathbf{e}_j^T$, c.f., [38, Def. 1.2].

³Historically speaking, (1) is called the s-stress function [48], interested reader is referred to our previous work for a short survey [22].

⁵Finding uniform bounds on $\mathcal{R}_\Omega^* \mathcal{R}_\Omega$, e.g., analogy of Lemma C.3, C.5 is challenging. While treating it as a sub-Gaussian quadratic form and applying the ‘suprema of chaos’ inequality [56] as in [57] [58] might yield a similar tangent space eigenvalue lower bound to [20, Lemma 10], the upper bound for replacing Lemma C.5 remains too loose.

pseudo gradient descent does not exhibit strong convergence in the sample-limited regime when compared to (1), despite its theoretical error contraction rate resembling that of the classic Riemannian Gradient Descent for Low-rank Matrix Completion (LRMC) [59].

B. Major Contributions

By introducing Burer-Monteiro factorization into (3), we have

$$\min_{\mathbf{P} \in \mathbb{R}^{n \times r}} f(\mathbf{P}) = \frac{1}{p} \langle \mathcal{R}_\Omega(\mathbf{P}\mathbf{P}^T - \mathbf{G}^*), \mathbf{P}\mathbf{P}^T - \mathbf{G}^* \rangle, \quad (4a)$$

$$\hat{\nabla} f(\mathbf{P}) = \frac{2}{p} \mathcal{R}_\Omega(\mathbf{P}\mathbf{P}^T - \mathbf{G}^*)\mathbf{P}, \quad (4b)$$

which, can be viewed as optimizing \mathbf{P} over a quotient manifold. Compared with [1], our major contributions are three fold:

- We analyze the contraction behavior when using (4b) to perform Projected GD (PGD), starting from a surrogate returned by a recent proposed spectral estimator [1] [23, Lemma 5.6] called One-step MDS (OS-MDS). This routine is referred to as the Asymmetric Projected Gradient Descent (APGD), where the projection step enforces iteration to stay incoherent, similar to the setup in [35]. We show a near linear convergence toward the ground truth of the APGD iteration can be established given $\mathcal{O}(\mu^2 r^3 \kappa^2 n \log n)$ random distance samples by constructing standard regularity condition w.r.t. the pseudo gradient direction.
- We provide two new uniform estimates for controlling two types of the non-tangent space residual during iteration in inner product form, namely, Lemma B.1 and B.2, thereby replacing the random graph lemma used in classic non-convex LRMC tasks. These bounds are developed based on a celebrated sharp result by Bandeira and van Handel [60], also the separation trick originated from Bhojanapalli and Jain [61], substantially different with the one used in our previous work [22, Lemma B.2].
- We present numerical comparison between the OS-MDS initialized un-regularized s-stress (1) and APGD with vanilla Barzilai-Borwein stepsize over synthetic point set. While the APGD is poorly behaved and appears to possess practical significance only in the near-asymptotic region, phenomena analogous to the role of incoherence restrictions in non-convex LRMC [62, Ch. 2] are observed. This raises interesting questions on the design principle of non-convex matrix recovery strategies under non-orthonormal, non-sub-Gaussian, and ill-conditioned sample basis – is EDMC a special case?

Organization: In Section II we provide a more detailed background and model setup. We state our main theorem and two important lemmas that control the initialization error of OS-MDS and contraction behavior of APGD in Section II-A. The proofs are referred to the Appendix. Section III contains the aforementioned numerical result and the manuscript is concluded with a discussion in Section IV.

Notation: \mathbf{y} , \mathbf{Y} stands for column vectors and matrices. Superscript $(\cdot)^*$ emphasize the ground truth. $\mathbf{1}$, $\mathbf{0}$, \mathbf{I} is the all

ones, all zeros vector, and the identity matrix. \mathbf{Y}_{ij} , $\text{diag}(\mathbf{Y})$, and $\text{diag}(\mathbf{y})$ is the (i, j) -th entity, column vector formed by the diagonal elements of \mathbf{Y} , and diagonal matrix formed by \mathbf{y} , respectively. $\mathbf{Y}_{\cdot, k} / \mathbf{Y}_{k, \cdot}^T$ stands for the k -th column/row of \mathbf{Y} . $\text{Od}(\mathbf{Y})$ means a matrix obtained by nullifying the diagonal of \mathbf{Y} . \mathcal{F}^* stands for the adjoint of a linear operator \mathcal{F} , and \mathcal{I} denotes the identity operator. \circ is the Hadamard product. $\|\mathbf{Y}\|$, $\|\mathbf{Y}\|_F$, $\|\mathbf{Y}\|_\infty$, $\|\mathbf{Y}\|_{2, \infty}$, $\|\mathbf{Y}\|_*$ stand for the spectral, Frobenius, entry-wise l_∞ , row-wise $l_{2, \infty}$, and nuclear norm of \mathbf{Y} . $\mathcal{S}(n)$ denotes the set of symmetric matrix in $\mathbb{R}^{n \times n}$, and $O(r)$ stands for the r dimensional orthogonal group. $\|\mathbf{y}\|_2$, $\|\mathbf{y}\|_\infty$ is the vector l_2 , l_∞ norm. $C, c > 0$ are universal constants that may differ from line to line. We retain $\beta > 2$ for expression like $n^{1-\beta}$, and C_β denotes a constant that dependent with β . $a \lesssim b$ and $a \gtrsim b$ stands for $a < Cb$ and $a > Cb$, respectively. $\mathbf{Y} \succcurlyeq \mathbf{0}$ means that \mathbf{Y} is PSD.

II. MATHEMATICAL SETUP AND MAIN RESULT

Let $\mathbf{P}^* = [\mathbf{p}_1^*, \dots, \mathbf{p}_n^*]^T \in \mathbb{R}^{n \times r}$ be the ground truth point set relative position and assume it has full column rank. The following non-convex QCQP (Quadratically Constrained Quadratic Programming) is usually referred to be the EDMC problem

$$\begin{aligned} & \text{find } \mathbf{G} \\ & \text{s.t. } \mathbf{G}_{ii} + \mathbf{G}_{jj} - 2\mathbf{G}_{ij} = \mathbf{D}_{ij}^*, (i, j) \in \Omega, \\ & \mathbf{G}\mathbf{1} = \mathbf{0}, \mathbf{G} \succcurlyeq \mathbf{0}, \text{rank}(\mathbf{G}) = r. \end{aligned} \quad (5)$$

Where $\mathbf{D}_{ij}^* = d_{ij}^{*2} = \|\mathbf{p}_i^* - \mathbf{p}_j^*\|_2^2 = \langle \mathbf{P}^* \mathbf{P}^{*T}, \boldsymbol{\omega}_\alpha \rangle$ denotes the (i, j) -th element in the ground truth EDM, and $\boldsymbol{\omega}_\alpha = (\mathbf{e}_i - \mathbf{e}_j)(\mathbf{e}_i - \mathbf{e}_j)^T$ is the so-called EDM basis. $\Omega \subset \mathbb{I} := \{(i, j) : i \leq i < j \leq n\}$ ⁶, and \mathbf{G} denotes the Gram matrix formed by $\mathbf{P}\mathbf{P}^T$. Obviously, the absolute configuration of points is lost and we can only recover \mathbf{P}^* up to translation, rotation, and reflection. The translation is removed by only considering self-centered point set⁷. The rotation and reflection ambiguity gives rise to a group synchronization problem over $O(r)$, and we use the solution of the orthogonal Procrustes problem to define the distance between \mathbf{P} and \mathbf{P}^*

$$\text{dist}(\mathbf{P}, \mathbf{P}^*)^2 = \|\Delta\|_F^2 := \min_{\boldsymbol{\psi} \in O(r)} \|\mathbf{P} - \mathbf{P}^* \boldsymbol{\psi}\|_F^2, \quad (6)$$

and the solution of (6) is denoted as $\boldsymbol{\psi}^*$. It satisfies $\mathbf{P}^T \mathbf{P}^* \boldsymbol{\psi}^* \succcurlyeq \mathbf{0}$ and $\Delta^T \mathbf{P}^* \boldsymbol{\psi}^* \in \mathcal{S}(r)$ [54, Lemma 6]. We also let Δ and $\boldsymbol{\psi}^*$ inherit any super/sub-script of \mathbf{P} , i.e., $\text{dist}(\mathbf{P}^{(\cdot)}, \mathbf{P}^*) = \|\Delta^{(\cdot)}\|_F = \|\mathbf{P}^{(\cdot)} - \mathbf{P}^* \boldsymbol{\psi}^{*(\cdot)}\|_F$.

The forward and inverse EDM mapping is needed to explicitly define the sample operator in (2), we restate them below

$$g(\mathbf{G}) := \text{diag}(\mathbf{G})\mathbf{1}^T + \mathbf{1}\text{diag}(\mathbf{G})^T - 2\mathbf{G}, \quad (7)$$

$$g^+(\mathbf{D}) := -\frac{1}{2}\mathbf{J}\mathbf{D}\mathbf{J}, \mathbf{J} = \mathbf{I} - \frac{1}{n}\mathbf{1}\mathbf{1}^T. \quad (8)$$

The ground truth EDM is sampled by the symmetric Bernoulli rule, that is $\Omega := \{(i, j) : \delta_\alpha = 1, \alpha \in \mathbb{I}\}$, where δ_α is a list

⁶Since the EDM is a symmetric and hollow matrix, we can omit its diagonal and only sample the upper triangle sub-matrix, which is referred to as the symmetric sampling later.

⁷W.l.o.g., we can always assume $\mathbf{P}^{*T}\mathbf{1} = \mathbf{0}$, and all considered point sets are in \mathcal{S}_c^n . That is, the identity operator \mathcal{I} used in this work actually denotes $\mathcal{I}_{\{\mathbf{1}\}^\perp}$. We abuse $\mathcal{I} = \mathcal{I}_{\{\mathbf{1}\}^\perp}$ for notation simplicity, one may also use different geometry centers, c.f., [63].

Algorithm 1 APGD

Require: Pseudo-gradient $\hat{\nabla}f(\mathbf{P})$ as in (4b), sampled distances $\mathcal{P}_\Omega \mathbf{D}^*$.

1: Initial APGD by OS-MDS as in [1] [23]

$$\hat{\mathbf{P}}\hat{\mathbf{P}}^T = \mathcal{T}_r \left[-\frac{1}{2p} \mathbf{J}(\mathcal{P}_\Omega \mathbf{D}^*) \mathbf{J} \right], \mathbf{P}_1 = \mathcal{P}_I(\hat{\mathbf{P}}),$$

where \mathcal{P}_I is defined by (14).

2: **for** $k = 1, 2, \dots$ **do**

3: $\mathbf{P}_{k+1} = \mathbf{P}_k - \frac{2\eta}{p} g^+ \mathcal{P}_\Omega(g(\mathbf{P}_k \mathbf{P}_k^T) - \mathbf{D}^*) \mathbf{P}_k$.

4: $\mathbf{P}_{k+1} = \mathcal{P}_I(\mathbf{P}_{k+1})$.

5: **end for**

6: **return** \mathbf{P}_k

of i. i. d. 0/1 Bernoulli random variables with $\mathbb{P}(\delta_\alpha = 1) = p$. Let \mathcal{P}_Ω denote the symmetric sample operator

$$\mathcal{P}_\Omega(\mathbf{D}) := \sum_{\alpha \in \mathbb{I}} \delta_\alpha (\langle \mathbf{D}, \mathbf{e}_i \mathbf{e}_j^T \rangle \mathbf{e}_i \mathbf{e}_j^T + \langle \mathbf{D}, \mathbf{e}_j \mathbf{e}_i^T \rangle \mathbf{e}_j \mathbf{e}_i^T). \quad (9)$$

A list of works [42] [63] [64] shows that by restricting \mathcal{I} onto the centered subspace $\mathcal{S}_c^n := \{\mathbf{A} : \mathbf{A}\mathbf{1} = \mathbf{0}, \mathbf{A} \in \mathcal{S}(n)\}$ and form $\mathcal{I}_{\{1\}^\perp}$, the following decomposition holds over \mathcal{S}_c^n

$$\begin{aligned} \mathcal{I}_{\{1\}^\perp}(\cdot) &:= g^+ g(\cdot) = -\frac{1}{2} \sum_{\alpha \in \mathbb{I}} \langle \cdot, \boldsymbol{\omega}_\alpha \rangle \mathbf{J}(\mathbf{e}_i \mathbf{e}_j^T + \mathbf{e}_j \mathbf{e}_i^T) \mathbf{J} \\ &= \sum_{\alpha \in \mathbb{I}} \langle \cdot, \boldsymbol{\omega}_\alpha \rangle \boldsymbol{\nu}_\alpha, \end{aligned} \quad (10)$$

and $\mathcal{I}_{\{1\}^\perp}(\mathbf{A}) = \mathbf{A}$ if $\mathbf{A} \in \mathcal{S}_c^n$. They call $\boldsymbol{\nu}_\alpha := -\frac{1}{2} \mathbf{J}(\mathbf{e}_i \mathbf{e}_j^T + \mathbf{e}_j \mathbf{e}_i^T) \mathbf{J}$ the dual-basis of $\boldsymbol{\omega}_\alpha$ [42]. From (10), we find the explicit expression of the pre-conditioned sample operator \mathcal{R}_Ω

$$\mathcal{R}_\Omega(\cdot) := g^+ \mathcal{P}_\Omega g(\cdot) = \sum_{\alpha \in \mathbb{I}} \delta_\alpha \langle \cdot, \boldsymbol{\omega}_\alpha \rangle \boldsymbol{\nu}_\alpha. \quad (11)$$

Under the symmetric Bernoulli model with parameter p , we have $\mathbb{E} \frac{1}{p} \mathcal{R}_\Omega = \mathbb{E} \frac{1}{p} \mathcal{R}_\Omega^* = \mathcal{I}$. Finally, let \mathcal{Q}_Ω be defined as

$$\mathcal{Q}_\Omega(\cdot) := \mathcal{P}_\Omega g(\cdot) = \sum_{\alpha \in \mathbb{I}} \delta_\alpha \langle \cdot, \boldsymbol{\omega}_\alpha \rangle (\mathbf{e}_i \mathbf{e}_j^T + \mathbf{e}_j \mathbf{e}_i^T). \quad (12)$$

A. Main Result

We are now ready to state our main result. Assume that \mathbf{P}^* satisfies the standard incoherence condition with $1 \leq \mu \leq \frac{n}{r}$, namely, let $\mathbf{P}^* \mathbf{P}^{*T} = \mathbf{U}^* \boldsymbol{\Sigma}^* \mathbf{U}^{*T}$ denotes its rank r thin Singular Value Decomposition (SVD), we have

$$\|\mathbf{U}^*\|_{2,\infty} \leq \sqrt{\frac{\mu r}{n}}, \|\mathbf{P}^*\|_{2,\infty} \leq \sqrt{\frac{\mu r \sigma_1^*}{n}}, \quad (13)$$

where $\sigma_i^* = \boldsymbol{\Sigma}_{ii}^*$, and let $\kappa = \sigma_1^*/\sigma_r^*$. The proposed APGD iteration is listed above as Algorithm 1, where $\mathcal{P}_I(\mathbf{P}_k)$ is defined as the following trimming step to enforce incoherence

$$\mathcal{P}_I(\mathbf{P}_k(i, :)) = \begin{cases} \mathbf{P}_k(i, :), & \text{if } \|\mathbf{P}_k(i, :)\|_2 \leq \sqrt{\frac{\mu r \sigma_1^*}{n}} \\ \frac{\mathbf{P}_k(i, :)}{\|\mathbf{P}_k(i, :)\|_2} \sqrt{\frac{\mu r \sigma_1^*}{n}}, & \text{otherwise} \end{cases} \quad (14)$$

Where $\mathbf{Y}(i, :)$ stands for the i -th row of \mathbf{Y} , and \mathcal{T}_r denotes the rank r SVD truncation.

Theorem II.1. Under the above set up, let $p \gtrsim C_\beta \frac{\mu^2 r^3 \kappa^2 \log n}{n}$. For any $k \geq 1$, i.e., Line 1 to Line 5 of Algorithm 1, we have

$$\|\Delta_k\|_F^2 \leq (1 - \eta')^{k-1} \frac{\sigma_r^*}{c_c}, \quad (15)$$

holds with probability at least $1 - cn^{1-\beta} - n^{2-\beta}$. Where $0 < \eta' \leq \frac{1}{336c_I \mu r}$, $c_c = \frac{80}{7}$, and Δ_k refers substituting \mathbf{P}_k into (6). To reach ς stationary point, i.e., $\|\Delta_k\|_F^2 / \|\Delta_0\|_F^2 \leq \varsigma$, APGD needs around $336c_I \mu r \log(\frac{1}{\varsigma})$ iterations.

The proof of Theorem II.1 is developed based on the following two lemmas, which describe the behavior of APGD inside the incoherence and contraction regions (RIC) \mathcal{B} , defined below

$$\mathcal{B} := \{\mathbf{P} : \|\Delta\|_{2,\infty} \leq \sqrt{\frac{c_I \mu r \sigma_1^*}{n}}, \|\Delta\|_F^2 \leq \frac{\sigma_r^*}{c_c}\}, c_I > 4.$$

Where the lower bound on c_I comes from $\|\Delta\|_{2,\infty} \leq \|\mathbf{P}\|_{2,\infty} + \|\mathbf{P}^*\|_{2,\infty} \leq 2\|\mathbf{P}^*\|_{2,\infty}$ by our parameter setting in the incoherence projection step (14).

Lemma II.1. The RIC region \mathcal{B} can be entered (i.e., $k = 1$, Line 1 in Algorithm 1) by using a spectral initialization followed by incoherence projection \mathcal{P}_I . That is,

$$\hat{\mathbf{P}}\hat{\mathbf{P}}^T = \mathcal{T}_r \left[-\frac{1}{2p} \mathbf{J}(\mathcal{P}_\Omega \mathbf{D}^*) \mathbf{J} \right], \mathbf{P}_1 = \mathcal{P}_I(\hat{\mathbf{P}}),$$

satisfies $\mathbf{P}_1 \in \mathcal{B}$ with probability at least $1 - n^{1-\beta}$, provided with $p \gtrsim C_\beta \frac{\mu^2 r^3 \kappa^2 \log n}{n}$.

Proof. Please see Appendix A. \square

Lemma II.2. Under the set up of Theorem II.1, inside the RIC \mathcal{B} , we have the following update rule for $k \geq 1$ (i.e. Line 2 to Line 5 in Algorithm 1)

$$\mathbf{P}_{k+1} = \mathcal{P}_I(\mathbf{P}_k - \frac{2\eta}{p} \mathcal{R}_\Omega(\mathbf{P}_k \mathbf{P}_k^T - \mathbf{G}^*) \mathbf{P}_k),$$

satisfies

$$\|\Delta_{k+1}\|_F^2 \leq (1 - \frac{\eta \sigma_r^*}{2}) \|\Delta_k\|_F^2,$$

with probability at least $1 - cn^{1-\beta} - n^{2-\beta}$, provided with $p \gtrsim C_\beta \frac{\mu^2 r^2 \kappa^2 \log n}{n}$, and $0 < \eta \leq \frac{1}{168\sigma_1^* c_I \mu r \kappa}$.

Proof. Please see Appendix B-A. \square

B. Proof of Theorem II.1

By our setting of parameters, (15) is a direct corollary of Lemma II.1 and Lemma II.2. The interval on η' comes from calculating $\frac{\eta \sigma_r^*}{2}$ with the step size η determined in Appendix B-A. What remains is to count iteration complexity using (15). Suppose choosing the largest possible $\eta' = \frac{1}{336c_I \mu r}$, we need to show $(1 - \frac{1}{336c_I \mu r})^{k_0-1} \leq \varsigma$, it requires

$$k_0 \geq \log(1/\varsigma) / \log\left(\frac{336c_I \mu r}{336c_I \mu r - 1}\right) + 1,$$

which approximately on the order of $\mathcal{O}(336c_I \mu r \log(1/\varsigma))^8$, concluding the proof. \square

Remark II.1. It is worth noting that the requirement on p in Lemma II.2, i.e., the establishment of regularity condition for the pseudo gradient, is of the same order in κ , μ , r , and n as its counterpart in classic LRMC theory [35, Lemma 3]. This observation leads us to conjecture that our techniques might be applied to tighten the estimate by Tasissa and Lai [20]. Meanwhile, the sample complexity for the OS-MDS is slightly

⁸Recall $\frac{1}{x+1} \leq \ln(\frac{x+1}{x}) = \int_x^{x+1} \frac{1}{t} dt \leq \frac{1}{x}$ for $0 < x < \infty$.

Algorithm 2 APGD With BB StepSize

Require: Pseudo-gradient $\mathbf{p}_g^k = p \widehat{\nabla} f(\mathbf{P}_k)$, sampled distances

- $$\mathcal{P}_\Omega \mathbf{D}^*.$$
- 1: $\hat{\mathbf{P}}\hat{\mathbf{P}}^T = \mathcal{T}_r \left[-\frac{1}{2p} \mathbf{J}(\mathcal{P}_\Omega \mathbf{D}^*) \mathbf{J} \right]$, $\mathbf{P}^0 = \mathcal{P}_I(\hat{\mathbf{P}})$
 - 2: **for** $k = 0, 1, \dots, N$ **do**
 - 3: $\mathbf{P}^{k+1} = \mathbf{P}^k - \eta_k \mathbf{p}_g^k$, $\mathbf{P}^{k+1} = \mathcal{P}_I(\mathbf{P}^{k+1})$.
 - 4: $\mathbf{S}_{k+1} = \mathbf{P}^{k+1} - \mathbf{P}^k$, $\mathbf{D}_{k+1} = \mathbf{P}^{k+1} - \mathbf{p}_g^k$.
 - 5: **if** $\text{mod}(k, 2) == 0$ **then**
 - 6: $\eta_k^{BB} = \frac{\|\mathbf{S}_{k+1}\|_F^2}{\langle \mathbf{S}_{k+1}, \mathbf{D}_{k+1} \rangle}$
 - 7: **else**
 - 8: $\eta_k^{BB} = \frac{\langle \mathbf{S}_{k+1}, \mathbf{D}_{k+1} \rangle}{\|\mathbf{D}_{k+1}\|_F^2}$
 - 9: **end if**
 - 10: $\eta_k = \min(\eta_k^{BB}, \eta_{\max})$
 - 11: **end for**
 - 12: **return** \mathbf{P}^k
-

suboptimal in r compared with the best-known bound [65, Thm. 3.23]. The direct rank $d+2$ truncation of an EDM (i.e., the SVD-MDS) has been shown to be minimax sub-optimal in [49, Sec. IV]. Since the OS-MDS shares almost same empirical phase transition edge as the SVD-MDS [1], it suggests that the idea of using $\|\frac{1}{p} \mathcal{P}_\Omega \mathbf{D}^* - \mathbf{D}^*\|$ to construct spectral estimator might be overly conservative in practice.

III. NUMERICAL EXPERIMENTS

The algorithm tested here is slightly different from the theoretical routine listed in Theorem II.1 (cf. Algorithm 2), in which BB stepsize without line search is employed, as inherited from [62, Ch. 2]⁹. The performance of incoherent projection-free OS-MDS, OS-MDS initialized GD refinement on s-stress (denoted as OS-MDS-GD) is also reported in Fig. 1 for comparison, more details on them can be found in [1].

A. Implementation Details

The parameters in performing \mathcal{P}_I can be estimated from the observations

$$\hat{\sigma}_1^* = c_1 \sigma_1(\hat{\mathbf{P}}\hat{\mathbf{P}}^T), \hat{\mu} = c_2 \frac{n}{r \hat{\sigma}_1^*} \max_{(i,j) \in \Omega} \mathbf{D}_{ij}^*,$$

where Lemma C.6 guarantees the approximation behavior of $\hat{\sigma}_1^*$, and c_1, c_2 are the parameters to tune. Since the APGD is more analogous to an analytical process rather than an algorithm used for benchmarking, we assume throughout all experiments that σ_1^* and μ are perfectly known. Unless otherwise specified, the ground truth point set is generated by a standard Gaussian distribution with embedding dimension $r = 2$, and results presented here are obtained under $\eta_{\max} = 10$. Algorithm 2 is terminated once $\|\mathbf{p}_g^k\|_F \leq 1 \times 10^{-6}$ or the iteration number reaches $N = 1000$. In contrast, both the upper and lower safeguards, $\eta_{\max} = \frac{2}{p \sigma_1^* \mu r \kappa}$ and $\eta_{\min} = \frac{1}{2p \sigma_1^* \mu r \kappa}$, are adopted in Section III-D for better illustration of linear convergence. Please note that the calculation of $\mathbf{J}\mathbf{A}\mathbf{J}$ for $\mathbf{A} \in \mathbb{R}^{n \times n}$ can be conducted in $\mathcal{O}(n^2)$ flops, as it amounts

⁹The lower safeguard on BB stepsize is removed in most experiments, i.e., η_k is allowed to be negative. Compared with pure GD, we found such sporadically occurring gradient ascent can numerically improve overall global convergence in all tested scenarios (especially the protein tests in Section III-E). The upper safeguard is retained to ensure algorithmic stability when c_{IP} is large, c.f., (17).

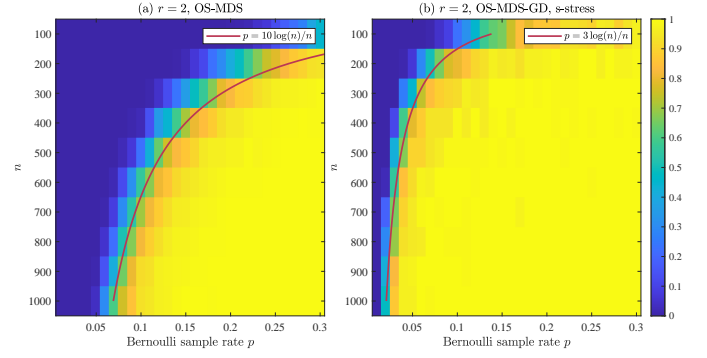


Fig. 1. The phase transition of regularization free OS-MDS and OS-MDS-GD when varying p and n [1]. We claim a success if the spectral error falls below 1 in (a), or the EDM recover rate is smaller than 10^{-3} in (b). For each (n, p) , the result is obtained by 100 independent trials.

to sequentially removing the mean value of \mathbf{A} 's columns and rows.

The spectral error (SE) and EDM recover rate (RE) defined below are used to evaluate the performance of OS-MDS, OS-MDS-GD, and the APGD.

$$\text{SE} := \frac{\|\hat{\mathbf{G}} - \mathbf{G}^*\|}{\|\mathbf{G}^*\|}, \text{RE} := \frac{\|\bar{\mathbf{D}} - \mathbf{D}^*\|_F}{\|\mathbf{D}^*\|_F},$$

where $\hat{\mathbf{G}}$ is the surrogate Gram matrix obtained from the spectral initialization without trimming, and $\bar{\mathbf{D}}$ is the EDM returned by either OS-MDS-GD or Algorithm 2. We record the trajectories of the following quantities during the execution of APGD.

$$g_1^k = 2 \|\mathcal{R}_\Omega(\mathbf{P}^k \mathbf{P}^{kT} - \mathbf{G}^*) \mathbf{P}^k\|_F, \quad (16a)$$

$$g_2^k = 2 \|\mathcal{R}_\Omega^*(\mathbf{P}^k \mathbf{P}^{kT} - \mathbf{G}^*) \mathbf{P}^k\|_F, \quad (16b)$$

$$r^k = \frac{\|\mathbf{P}^k \mathbf{P}^{kT} - \mathbf{G}^*\|_F}{\|\mathbf{G}^*\|_F}, \quad (16c)$$

where g_2^k can be viewed as the norm of the second term in the gradient of (4a), it cannot be computed unless direct access to \mathbf{G}^* is available. We conjecture that the limited numerical performance of APGD in the sample-limited regime can be attributed to at least three factors¹⁰: (i) the weakening of implicit regularization; (ii) the large residual between the pseudo-gradient and its population-level counterpart; (iii) the inconsistency between pseudo-gradient and the true gradient of (4a). These factors will be illustrated sequentially in the following sections.

B. Phase Transition Under Gaussian Point Set

The phase transition of APGD is plotted in Fig. 2, and we fit its edge using $p = 10 \log(n)/n$ curve. Interestingly, the incoherence projection becomes essential for achieving relatively robust performance, which bears a resemblance to the case in standard LRMC problems [34]. If one sets

$$\|\mathbf{P}_k(i, :)\|_2 \leq c_{IP} \sqrt{\frac{\mu r \sigma_1^*}{n}}, \quad (17)$$

in (14) with some $c_{IP} > 1$, the performance of APGD on Gaussian random point sets will be degenerated, as suggested by Fig. 2(b), (c), and (d). This observation indicates that the power of implicit regularization to maintain incoherence is weakened in the APGD case. More delicate evaluations are

¹⁰The second factor is believed to be the most dominant.

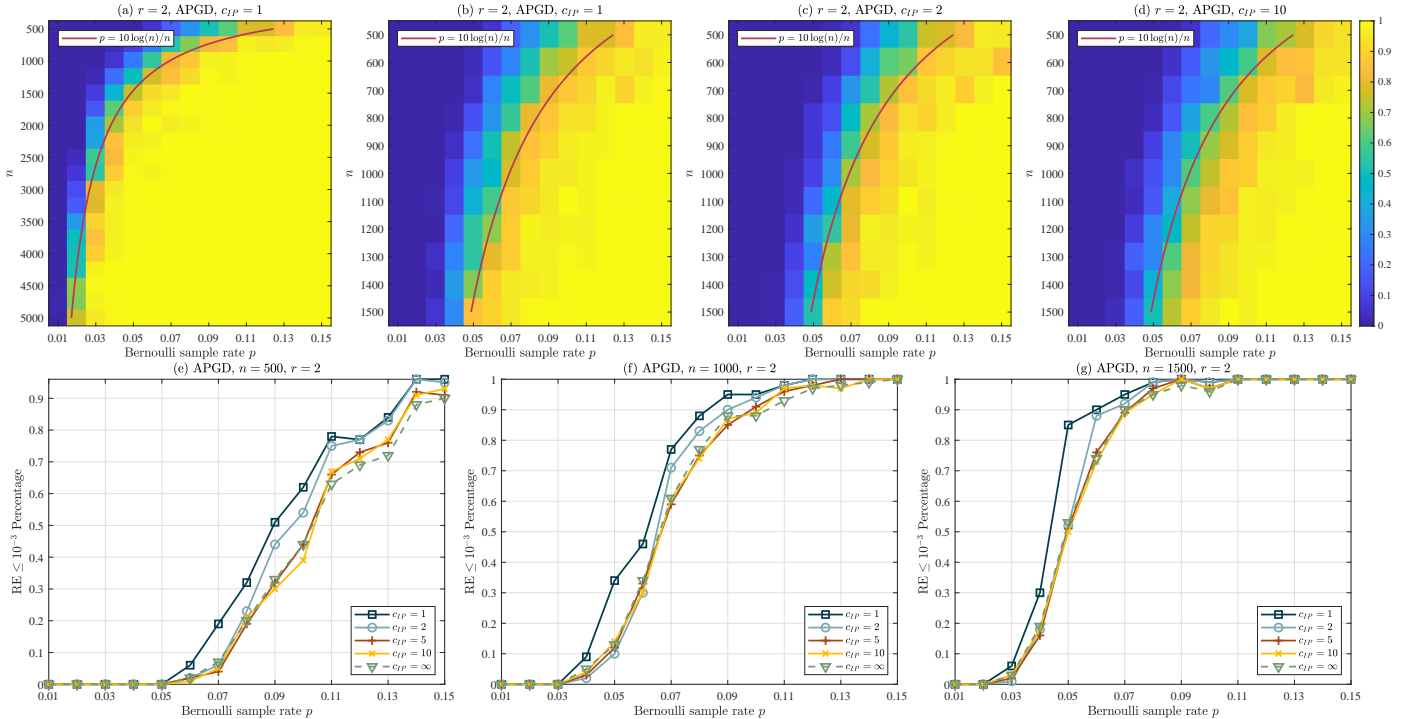


Fig. 2. (a) The phase transition of APGD when varying Bernoulli sample rate p and the number of points n . The result is obtained by 100 independent trials. To verify Theorem II.1, we claim a success if the EDM recover rate falls below 10^{-3} . In (b), (c), and (d), we vary the constant c_{IP} in (17) when performing incoherent projection, while all other parameters remain unchanged. Subplot (e), (f), and (g) show selected phase transition curves when $n = 500, 1000, 1500$ with c_{IP} varies.

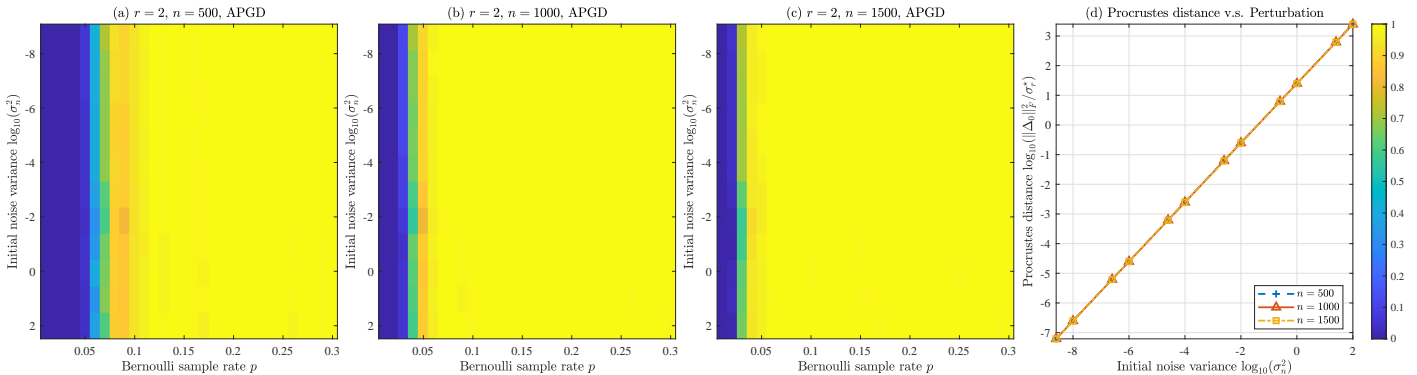


Fig. 3. The phase transition of APGD when varying Bernoulli sample rate p and the standard variance of perturbation white noise σ_n . A success is recorded if the EDM recover rate falls below 10^{-5} . In (a), (b), and (c), we change the number of points from $n = 500$ to $n = 1500$, with all other parameters fixed. (d) plots the relationship between normalized quotient distance $\|\Delta\|_F^2 / \sigma_r^*$ and the intensity of noise σ_n^2 .

carried out in Fig. 2(e), (f), and (g). This reveals that APGD can still converge when the trimming step is removed, yet larger c_{IP} gives rise to more oscillations and non-monotonicity in the transition curve, ultimately leading to broader transition interval measured by p .

By comparing Fig. 1(a) and Fig. 2(a), we find that the phase transition edge of APGD matches that of OS-MDS. This phenomenon confirms the prediction in Lemma II.2, and yet is quite unusual, as both non-convex Gaussian ensemble phase retrieval and structure-less LRMC do not necessarily rely on the spectral initialization to succeed [66] [67]. Since the proof roadmap in [67] indicates that the success of rescaled eigenspace alignment initialization relies on the implicit incoherent regularization ability of the original fourth-order polynomial-type cost function for LRMC, we infer that when this property is compromised, the algorithm may start to

behave selective on the quality of starting point. Alternatively, more dedicated initialization for APGD can somewhat improve the transition edge. However, the OS-MDS-GD strategy exhibits empirical convergence when started inside a slack region around the ground truth as depicted in Fig. 1(b), even without any incoherence projection.

C. Phase Transition Under Random Perturbation

A randomly perturbed initialization is deployed in this section to verify the existence of restricted strong convexity in the pseudo-gradient direction. It reads

$$\mathbf{P}_0 = \mathbf{J}(\mathbf{P}^* + \sigma_n \mathbf{E}_n) \in \mathbb{R}^{n \times r},$$

where \mathbf{E}_n is a Gaussian random matrix with $[\mathbf{E}_n]_{ij} \sim \mathcal{N}(0, 1)$ and \mathbf{P}^* is generated from a uniform distribution over the hypercube $[-0.5, 0.5]^r$. The noise level σ_n is varied from 5×10^{-5} to 10. The iteration will be terminated if $\|\mathbf{p}_g^k\|_F \leq$

TABLE I
PARAMETERS OF TEST PROTEINS

Protein	n	μ	κ	$\mu\kappa$	Protein	n	μ	κ	$\mu\kappa$	Protein	n	μ	κ	$\mu\kappa$
IAX8	1003	1.8653	2.9567	5.5154	IKDH	2846	2.2583	2.7716	6.2592	IBPM	3671	1.9289	4.1451	7.9956
IRGS	2015	2.0494	4.3926	8.8733	IMQQ	5681	2.1796	3.3211	7.2389	IYGP	13488	1.6348	3.8056	6.2218
ITIM	3740	1.3297	4.9413	6.5706	ITOA	4292	1.6424	5.3534	8.7929	I17W	8629	1.8189	20.5725	37.4202

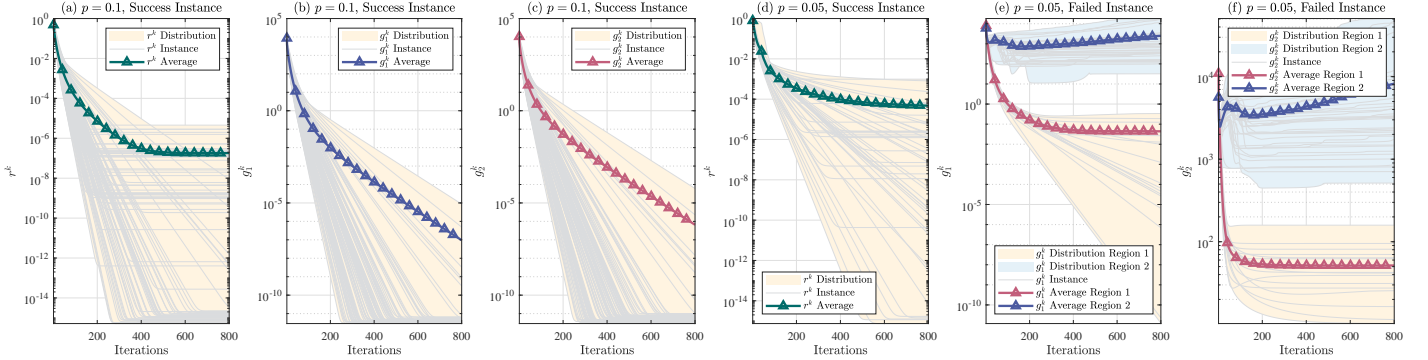


Fig. 4. Trajectories of all three quotas in (16) while fixing $n = 1500$. The result is obtained from 100 independent trials. (a), (d) shows the tendency of r^k in selected succeed instances (96% when $p = 0.1$, 47% when $p = 0.05$). (b), (c) plots the corresponding g_1^k , g_2^k when $p = 0.1$. (e), (f) contains the records of g_1^k and g_2^k of selected failed instances (53% when $p = 0.05$). These trajectories can be divided into two groups (17% in region 1, 36% in region 2).

10^{-8} , while all other parameters follow the same setup as in Fig. 2(b). Since the perturbation can be relatively small, we claim a success if $\text{RE} \leq 10^{-5}$, and the resulting phase transitions are plotted in Fig. 4 for $n = 500, 1000, 1500, r = 2$, where $\|\Delta_0\|_F^2$ refers to $\text{dist}(\mathbf{P}_0, \mathbf{P}^*)^2$. Around $\sigma_n \leq 0.1$, i.e., inside the region where $\|\Delta_0\|_F^2 \leq \sigma_r^*$ according to Fig. 2(d), these plots depict that the convergence of APGD becomes sensitive primarily to the sample complexity. As $p \rightarrow 1$, the $\nabla f(\mathbf{P})$ reduces to the gradient direction of the vanilla matrix factorization problem, which is known to exhibit local restricted strong convexity [52, Thm. 5]. Therefore, Fig. 3 also demonstrates the lower bound on p necessary for this approximation to hold.

However, this dependence on p is sub-optimal compared to the performance achieved by either OS-MDS-GD or trace minimization methods [20, Sec. IV] [31, Sec. 5], indicating that the stabilization of pseudo gradient¹¹ needs more random samples to guarantee, even though Lemma II.2 predicts that the establishment of regularity condition should require the same order of sample complexity as in classical LRMC problems. Moreover, it is noteworthy that OS-MDS cannot achieve $\|\Delta_0\|_F^2 \leq \sigma_r^*$ with high probability at the sample configurations $\{(n, p) : (500, 0.08), (1000, 0.05), (1500, 0.04)\}$, which is why we allow Algorithm 2 to take negative stepsize, thereby facilitating global optimization.

D. Iteration Trajectory

A special instance of experiments in Section III-B is investigated in greater detail. We consider $(n, p) = (1500, 0.1)$, $(n, p) = (1500, 0.05)$, and plot the convergence trajectories measured by (16) in Fig. 4. When $p = 0.1$, 96% of the trials successfully recover the EDM. The corresponding trajectories of r^k , g_1^k , and g_2^k are presented in Fig. 4(a), (b), and (c) respectively, where exact linear convergence is observed after

¹¹More specifically, ensuring the upper bound on Eq. (23) in Appendix B-B.

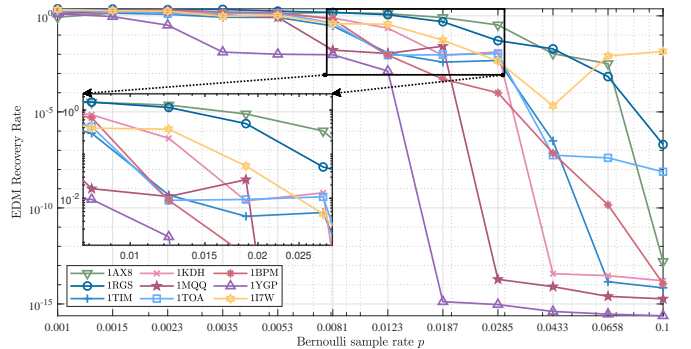


Fig. 5. The phase transition measured by EDM recovery rate of APGD when varying protein type and Bernoulli sample rate p , while fixing $r = 3$. Detailed parameters for each protein are listed in Table I. The results are averaged over 5 independent trials.

a few iterations, as indicated by the gray lines. Moreover, the pseudo gradient and g_2^k demonstrated nearly identical behavior. When $p = 0.05$, 47% of the recordings are categorized to be successful¹², with their r^k shown in Fig. 4(d). Intriguing phenomena emerge when analyzing the other failed 53%, as illustrated in Fig. 4(e), (f), where g_1^k and g_2^k no longer coincide. In about 17% of all trials, the pseudo gradient tends to converge, whereas the corresponding g_2^k does not. This observation might uncover a potential factor underlying the degraded numerical performance of APGD, i.e., the consistency between pseudo gradient and the real gradient of (4a) (up to trivial rescale) demands an unreasonably large number of samples to be reliably ensured.

E. Protein Test

Phase transition tests on nine proteins downloaded from the Protein Data Bank [68] are presented in Fig. 5 to evaluate the real-world performance of APGD, as well as the impact

¹²This clearly highlights the performance degradation caused by imposing the lower safeguard η_{\min} . Also, the succeeded instances of g_1^k and g_2^k when $p = 0.05$ resemble those in Fig. 4(b), (c), and thus omitted here.

of condition number κ and coherence parameter μ . Similar experiments but under the unit ball sample model and challenging noisy observations settings can be found in [9, Sec. 5.3]. Prior to processing, solvent molecules and chelated metal ions were removed from the datasets. The resulting parameters n , μ , and κ are reported in Table I.

Non-monotonic trends in sample complexity p w.r.t. n are observed, e.g., although the atom number of 1I7W is approximately three times larger than that of 1KDH, the phase transition for 1KDH occurs at a significantly lower sampling ratio. This phenomenon is attributed to the large condition number associated with the 1I7W configuration, which both suppresses the BB stepsize and increases the sample complexity required for global recovery, as predicted by Theorem II.1. Furthermore, the performance of Algorithm 2 appears sensitive to the product $\mu\kappa$, since the curves of 1AX8 versus 1RGS, and 1TIM versus 1TOA exhibit similar “reversal”¹³, due to small changes in their corresponding $\mu\kappa$ values.

IV. CONCLUSION AND DISCUSSION

By paralleling matrix factorization type incoherent LRMC technique, this manuscript analyzes the quotient variant of a recent proposed Iterative Fast Hard Thresholding procedure for Euclidean Distance Matrix Completion [23], namely, the Asymmetric Projected Gradient Descent. By leveraging the nuclear norm splitting trick in [61] [69] [70] [71], and employing the sharp bound on the second largest eigenvalue of a Erdős-Rényi graph [60], we provide refined analysis on different components of the residual, and further establish the regularity condition. This, in turn, enables the first characterization of near-linear convergence behavior for matrix factorization-based EDMC algorithms. Numerical experiments corroborate the predicted convergence behavior of the pseudo gradient descent method in rich-sample regimes, yet raise questions on general design principle and the adequacy of classic incoherence notion in the context of non-convex EDMC techniques, we list two of them below.

- Since the EDM basis shares a similar support pattern with $\mathbf{e}_i \mathbf{e}_j^T$, [20] introduced the incoherence w.r.t. ω_α and ν_α to measure the concentration of information in \mathbf{G}^* . While such definition, c.f., [41, Def. 2], can be deduced from classical incoherence assumption up to trivial rescale by resorting to [23, Lemma A.4], this does not fully account for the observed performance gap between trace minimization and VGD applied to (1). In the context of Hankel Matrix Completion (HMC), incoherence is satisfied if the minimum wraparound distance between spikes remains non-vanishing [72, Sec. III-A], and both EMaC (convex approach to HMC) and PGD-like algorithms [45] [73] are observed to succeed even without strict separation. But for EDMC, which property of the point set govern the problem’s tractability?
- According to [41], the dual basis approach provides a way to construct a preconditioned sampling operator

for non-orthonormal, discrete, and ill-conditioned sensing bases. Corresponding modifications of the Golfing Scheme, IFHT, and PDG frameworks achieve theoretical success for EDMC, yet the practical significance of the latter two severely suffers. While it is acknowledged that under the orthogonal setting, numerical performance of similar strategies relies on implicit regularization, which characteristic of the sample basis determines its strength?

ACKNOWLEDGMENT

The authors would like to thank Abiy Tasissa for insightful discussion and help in proofreading the manuscript.

APPENDIX A

PROOF OF LEMMA II.1

This is a direct use of Lemma C.6. Notice that

$$\begin{aligned} \|\Delta_1\|_F^2 &:= \|\mathcal{P}_I(\hat{\mathbf{P}} - \mathbf{P}^* \psi^*)\|_F^2 \stackrel{(i)}{\leq} \|\hat{\mathbf{P}} - \mathbf{P}^* \psi^*\|_F^2 \\ &\stackrel{(ii)}{\leq} \frac{1}{2(\sqrt{2}-1)\sigma_r^*} \|\hat{\mathbf{P}}\hat{\mathbf{P}}^T - \mathbf{P}^* \mathbf{P}^{*T}\|_F^2 \\ &\stackrel{(iii)}{\leq} \frac{r}{2(\sqrt{2}-1)\sigma_r^*} \|\hat{\mathbf{P}}\hat{\mathbf{P}}^T - \mathbf{P}^* \mathbf{P}^{*T}\|^2 \\ &\stackrel{(iv)}{\leq} \frac{r\epsilon^2 \sigma_1^{*2}}{2(\sqrt{2}-1)\sigma_r^*} \stackrel{(v)}{\lesssim} \frac{\sigma_r^*}{c_c}, \end{aligned}$$

where (i) uses the convexity of the set $\{\mathbf{P} : \|\mathbf{P}\|_{2,\infty} \leq \sqrt{\frac{c_I \mu r \sigma_1^*}{n}}\}$, see also [35, Lemma 11]. (ii) comes from [54, Lemma 6], and (iii) uses $\|\mathbf{A}\|_F^2 \leq r \|\mathbf{A}\|^2$ if $\text{rank}(\mathbf{A}) = r$. (iv) comes from Lemma C.6, and holds with probability at least $1 - n^{1-\beta}$ given $p \gtrsim \frac{C_\beta \mu^2 r^2 \log n}{\epsilon^2 n}$. Finally (v) by setting $\epsilon^2 \leq \frac{1}{C_\epsilon \kappa^2 r}$, where $C_\epsilon \gtrsim c_c$, concluding the proof. \square

APPENDIX B

PROOF OF LEMMA II.2

Recall the rank- r SVD of $\mathbf{G}^* = \mathbf{P}^* \mathbf{P}^{*T}$ is denoted as $\mathbf{U}^* \Sigma^* \mathbf{U}^{*T}$. The tangent space at \mathbf{G}^* are given by (18), and the projections onto it is denoted by $\mathcal{P}_\mathbb{T}$.

$$\mathbb{T} = T_{\mathbf{G}^*} \mathcal{S}_+^{r,n} = \{\mathbf{U}^* \mathbf{W}_1^T + \mathbf{W}_1 \mathbf{U}^{*T}\}, \quad (18a)$$

$$\mathcal{P}_\mathbb{T}(\mathbf{Y}) = \mathcal{P}_\mathbf{U} \mathbf{Y} + \mathbf{Y} \mathcal{P}_\mathbf{U} - \mathcal{P}_\mathbf{U} \mathbf{Y} \mathcal{P}_\mathbf{U}, \quad (18b)$$

where $\mathcal{P}_\mathbf{U} = \mathbf{U}^* \mathbf{U}^{*T}$, and $\mathbf{W}_1 \in \mathbb{R}^{n \times r}$ are arbitrary. Let $\hat{\nabla} f(\mathbf{P}) := \frac{p}{r} \mathcal{R}_\Omega(\mathbf{P} \mathbf{P}^T - \mathbf{G}^*) \mathbf{P}$ denote the pseudo gradient. We will also frequently use Lemma C.7 without explicitly referring to it.

A. Local Contraction With Re-sampling

It is meanwhile straightforward to prove the local contraction property by following the roadmap in, e.g., [35, App. D] [45, App. C] [73], given the following claim holds for the moment.

Claim B.1. *For a fix ground truth point set \mathbf{P}^* independent with Ω , uniformly for all $\mathbf{P} \in \mathbb{R}^{n \times r}$ inside the RIC \mathcal{B} , we have the following regularity condition holds*

$$\langle \hat{\nabla} f(\mathbf{P}), \Delta \rangle \geq \alpha \|\Delta\|_F^2, \quad (19a)$$

$$\|\hat{\nabla} f(\mathbf{P})\|_F^2 \leq \rho \|\Delta\|_F^2, \quad (19b)$$

$$\langle \hat{\nabla} f(\mathbf{P}), \Delta \rangle \geq \frac{\alpha}{2} \|\Delta\|_F^2 + \frac{\alpha}{2\rho} \|\hat{\nabla} f(\mathbf{P})\|_F^2, \quad (19c)$$

¹³That is, the phase transition for a protein with larger n occurs later than that for a protein with smaller n .

with probability at least $1 - cn^{1-\beta}$, provided with $p \gtrsim C_\beta \frac{\kappa^2 \mu^2 r^2 \log n}{\varepsilon^2 n}$. Where $\alpha = \frac{1}{2} \sigma_r^*$, $\rho = 84 \sigma_1^{*2} c_I \mu r$, and $\varepsilon \leq \frac{1}{10}$.

(19a) and (19b) will be proved in App. B-B and B-C, respectively. (19c) is a direct conclusion from combining (19a) and (19b). Therefore we have

$$\begin{aligned} \|\Delta_{k+1}\|_F^2 &\leq \|\mathbf{P}_{k+1} - \mathbf{P}^* \boldsymbol{\psi}_k^*\|_F^2 \\ &= \|\mathcal{P}_I(\mathbf{P}_k - \eta \hat{\nabla} f(\mathbf{P}_k) - \mathbf{P}^* \boldsymbol{\psi}_k^*)\|_F^2 \\ &\leq \|\mathbf{P}_k - \eta \hat{\nabla} f(\mathbf{P}_k) - \mathbf{P}^* \boldsymbol{\psi}_k^*\|_F^2 \\ &= \|\Delta_k\|_F^2 + \eta^2 \|\hat{\nabla} f(\mathbf{P}_k)\|_F^2 - 2\eta \langle \hat{\nabla} f(\mathbf{P}_k), \Delta_k \rangle \\ &\stackrel{(i)}{\leq} (1 - \eta\alpha) \|\Delta_k\|_F^2 + \eta(\eta - \frac{\alpha}{\rho}) \|\hat{\nabla} f(\mathbf{P}_k)\|_F^2 \\ &\stackrel{(ii)}{\leq} (1 - \eta\alpha) \|\Delta_k\|_F^2, \end{aligned} \quad (20)$$

(i) by using Claim B.1, and (ii) by setting $0 < \eta \leq \min\{\frac{1}{\alpha}, \frac{\alpha}{\rho}\} = \frac{1}{168 \sigma_1^* c_I \mu r \kappa}$, where we conclude the proof. \square

B. Restricted Strong Convexity: (19a)

The proof follows similar idea as in [22, App. B], but the asymmetry structure of the pseudo gradient requires very careful control of the residuals. We start from lower bounding the population level gradient. Let us denote $\mathbb{E} \hat{\nabla} f(\mathbf{P}) = 2(\mathbf{P}\mathbf{P}^T - \mathbf{G}^*)\mathbf{P}$, and $\bar{\mathbf{P}}^* = \mathbf{P}^* \boldsymbol{\psi}^*$, thus

$$\begin{aligned} A_1 &:= \langle \mathbb{E} \hat{\nabla} f(\mathbf{P}), \Delta \rangle = \langle \mathbf{P}\mathbf{P}^T - \mathbf{G}^*, \Delta \mathbf{P}^T + \mathbf{P} \Delta^T \rangle \quad (21) \\ &= \langle \Delta \bar{\mathbf{P}}^{*T} + \bar{\mathbf{P}}^* \Delta^T + \Delta \Delta^T, \Delta \bar{\mathbf{P}}^{*T} + \bar{\mathbf{P}}^* \Delta^T + 2\Delta \Delta^T \rangle \\ &\stackrel{(i)}{\geq} \frac{5}{8} \overbrace{\|\Delta \bar{\mathbf{P}}^{*T} + \bar{\mathbf{P}}^* \Delta^T\|_F^2}^{a^2} - 4 \overbrace{\|\Delta \Delta^T\|_F^2}^{b^2}, \\ &\stackrel{(ii)}{\geq} (\frac{5}{4} \sigma_r^* - 4 \|\Delta\|_F^2) \|\Delta\|_F^2, \end{aligned} \quad (22)$$

where (i) follows from opening up the inner product and using Cauchy-Schwarz, then followed by elementary inequality

$$a^2 + 2b^2 - 3ab \geq (1 - \frac{3\gamma^2}{2})a^2 + (2 - \frac{3}{2\gamma^2})b^2,$$

with $\gamma = \frac{1}{2}$. (ii) dues to the fact that $\|\Delta \Delta^T\|_F \leq \|\Delta\|_F^2$, and $\Delta^T \bar{\mathbf{P}}^* = \bar{\mathbf{P}}^{*T} \Delta$, i.e.,

$$\begin{aligned} \|\Delta \bar{\mathbf{P}}^{*T} + \bar{\mathbf{P}}^* \Delta^T\|_F^2 &= 2\|\bar{\mathbf{P}}^* \Delta^T\|_F^2 + \text{tr}(\bar{\mathbf{P}}^* \bar{\mathbf{P}}^{*T} \Delta \Delta^T) \\ &\geq 2\|\bar{\mathbf{P}}^* \Delta^T\|_F^2 \geq 2\sigma_r^* \|\Delta\|_F^2. \end{aligned}$$

We next upper bound the distortion between sampled gradient and its population version. For notation simplicity, let $\mathcal{H}_\Omega := \frac{1}{p} \mathcal{R}_\Omega - \mathcal{I}$ for the moment. For any \mathbf{P} , we have

$$\begin{aligned} A_2 &:= |\langle \hat{\nabla} f(\mathbf{P}) - \mathbb{E} \hat{\nabla} f(\mathbf{P}), \Delta \rangle| \\ &= |\langle \mathcal{H}_\Omega(\Delta \bar{\mathbf{P}}^{*T} + \bar{\mathbf{P}}^* \Delta^T + \Delta \Delta^T), \Delta \bar{\mathbf{P}}^{*T} + \bar{\mathbf{P}}^* \Delta^T + 2\Delta \Delta^T \rangle| \\ &\leq \underbrace{|\langle \mathcal{H}_\Omega(\Delta \bar{\mathbf{P}}^{*T} + \bar{\mathbf{P}}^* \Delta^T), \Delta \bar{\mathbf{P}}^{*T} + \bar{\mathbf{P}}^* \Delta^T \rangle|}_{L_1} \\ &\quad + 2 \underbrace{|\langle \mathcal{H}_\Omega(\Delta \bar{\mathbf{P}}^{*T} + \bar{\mathbf{P}}^* \Delta^T), \Delta \Delta^T \rangle|}_{L_{21}} + 2 \underbrace{|\langle \mathcal{H}_\Omega(\Delta \Delta^T), \Delta \Delta^T \rangle|}_{L_{22}} \\ &\quad + \underbrace{|\langle \mathcal{H}_\Omega^*(\Delta \bar{\mathbf{P}}^{*T} + \bar{\mathbf{P}}^* \Delta^T), \Delta \Delta^T \rangle|}_{L_3}. \end{aligned} \quad (23)$$

(23) is quite different from existing literature on non-convex matrix completion (e.g., [34] [35] [45] [22] [73] [44]). This asymmetry structure and heavy diagonal basis $\boldsymbol{\omega}_\alpha$ make driving universal bounds on L_{21} , L_{22} , L_3 challenging. Similar predicament will occur in the restricted smoothness part, causing the step size to be dependent on μ , r .

Bound on L_1 : Recall that $\Delta \bar{\mathbf{P}}^{*T} + \bar{\mathbf{P}}^* \Delta^T \in \mathbb{T}$, and

$$\left\| \frac{1}{p} \mathcal{P}_\mathbb{T} \mathcal{R}_\Omega \mathcal{P}_\mathbb{T} - \mathcal{P}_\mathbb{T} \right\| \leq \frac{\varepsilon_{L_1}}{c\kappa} < 1,$$

if $p \gtrsim C_\beta \frac{\kappa^2 \mu^2 r^2 \log n}{\varepsilon_{L_1}^2 n}$ by Lemma C.3. Thus for some $c > 4$

$$\begin{aligned} L_1 &= \langle (\frac{1}{p} \mathcal{P}_\mathbb{T} \mathcal{R}_\Omega \mathcal{P}_\mathbb{T} - \mathcal{P}_\mathbb{T})(\Delta \bar{\mathbf{P}}^{*T} + \bar{\mathbf{P}}^* \Delta^T), \Delta \bar{\mathbf{P}}^{*T} + \bar{\mathbf{P}}^* \Delta^T \rangle \\ &\leq \frac{\varepsilon_{L_1}}{c\kappa} \|\Delta \bar{\mathbf{P}}^{*T} + \bar{\mathbf{P}}^* \Delta^T\|_F^2 \\ &\leq \frac{4\sigma_1^* \varepsilon_{L_1}}{c\kappa} \|\Delta\|_F^2 \lesssim \varepsilon_{L_1} \sigma_r^* \|\Delta\|_F^2. \end{aligned} \quad (24)$$

Bound on L_{21} and L_{22} : We use the following sharp bound to handle L_{21} and L_{22} , its proof is deferred to App. D-A.

Lemma B.1. *Uniformly for all matrix \mathbf{A} , \mathbf{B} , \mathbf{C} , $\mathbf{D} \in \mathbb{R}^{n \times r}$, we have*

$$\begin{aligned} \left| \left\langle \left(\frac{1}{p} \mathcal{R}_\Omega - \mathcal{I} \right) (\mathbf{A} \mathbf{B}^T), \mathbf{C} \mathbf{D}^T \right\rangle \right| \\ \leq 2c_g \sqrt{\frac{n}{p}} \|\mathbf{A}\|_{2,\infty} \|\mathbf{B}\|_{2,\infty} \|\mathbf{C} \mathbf{D}^T\|_F, \end{aligned}$$

holds for some constant $c_g > 0$ with probability at least $1 - n^{1-\beta}$ given $p \gtrsim \frac{C_\beta \log n}{n}$.

Therefore, by the symmetric structure of $\Delta \bar{\mathbf{P}}^{*T} + \bar{\mathbf{P}}^* \Delta^T$, we have

$$\begin{aligned} L_{21} &\leq 8c_g \sqrt{\frac{n}{p}} \|\Delta\|_{2,\infty} \|\mathbf{P}^*\|_{2,\infty} \|\Delta\|_F^2 \\ &\stackrel{(i)}{\leq} 8c_g \sqrt{\frac{c_I \mu^2 r^2 \sigma_1^{*2}}{np}} \|\Delta\|_F^2 \stackrel{(ii)}{\lesssim} \varepsilon_{L_{21}} \sigma_r^* \|\Delta\|_F^2, \end{aligned} \quad (25)$$

where (i) uses the incoherence assumption on the ground truth and attractive region, i.e., $\|\Delta\|_{2,\infty} \leq \sqrt{\frac{c_I \mu r \sigma_1^*}{n}}$. (ii) by forcing $p \gtrsim C_\beta (\kappa^2 \mu^2 r^2) / (n \varepsilon_{L_{21}}^2)$. The same argument works for L_{22} , that is for $p \gtrsim C_\beta (\kappa^2 \mu^2 r^2) / (n \varepsilon_{L_{22}}^2)$, we have

$$\begin{aligned} L_{22} &\leq 8c_g \sqrt{\frac{n}{p}} \|\Delta\|_{2,\infty}^2 \|\Delta\|_F^2 \\ &\leq 8c_g \sqrt{\frac{c_I^2 \mu^2 r^2 \sigma_1^{*2}}{np}} \|\Delta\|_F^2 \lesssim \varepsilon_{L_{22}} \sigma_r^* \|\Delta\|_F^2. \end{aligned} \quad (26)$$

Bound on L_3 : This is slightly larger, and the ‘‘uniform’’ part crucially relies on the fact that \mathbf{P}^* is a fixed matrix. It seems hard to reinforce Lemma B.2 to hold uniformly over all rank r incoherent matrix \mathbf{B} . The proof is referred to App. D-B.

Lemma B.2. *Uniformly for all matrix \mathbf{A} , \mathbf{C} , $\mathbf{D} \in \mathbb{R}^{n \times r}$, $\mathbf{R} \in O(r)$, and some fix matrix $\mathbf{B} \in \mathbb{R}^{n \times r}$ independent with Ω , which satisfy $\mathbf{A}^T \mathbf{1} = \mathbf{0}$, $\mathbf{B}^T \mathbf{1} = \mathbf{0}$, we have*

$$\left| \left\langle \left(\frac{1}{p} \mathcal{R}_\Omega^* - \mathcal{I} \right) (\mathbf{A} \mathbf{R}^T \mathbf{B}^T), \mathbf{C} \mathbf{D}^T \right\rangle \right|$$

$$\leq \left(C \sqrt{\frac{\beta n \log n}{p}} \|\mathbf{A}\|_{2,\infty} \|\mathbf{B}\|_{2,\infty} \right) \|\mathbf{C}\mathbf{D}^T\|_F,$$

holds for some constant $C > 0$ with probability at least $1 - n^{1-\beta} - n^{2-\beta}$ given $p \gtrsim \frac{C_\beta \log n}{n}$.

Thus, by using the symmetric structure of $(\frac{1}{p}\mathcal{R}_\Omega - \mathcal{I})(\Delta\Delta^T)$, we have

$$\begin{aligned} L_3 &\leq 2 \left| \left\langle \left(\frac{1}{p}\mathcal{R}_\Omega^* - \mathcal{I} \right) (\Delta\psi^{*T}\mathbf{P}^{*T}), \Delta\Delta^T \right\rangle \right| \\ &\leq 2C \sqrt{\frac{\beta n \log n}{p}} \|\Delta\|_{2,\infty} \|\mathbf{P}^*\|_{2,\infty} \|\Delta\|_F^2 \\ &\leq 2C \sqrt{\frac{c_I \mu^2 r^2 \sigma_1^{*2} \log n}{np}} \stackrel{(i)}{\lesssim} \varepsilon_{L_3} \sigma_r^* \|\Delta\|_F^2, \end{aligned} \quad (27)$$

holds uniformly over all $\mathbf{P} \in \mathcal{B}$, where (i) by setting $p \gtrsim C_\beta \frac{\kappa^2 \mu^2 r^2 \log n}{\varepsilon_{L_3}^2 n}$.

Substituting (24), (25), (26), and (27) into (23), and set $\varepsilon_{L_1} = \varepsilon_{L_{21}} = \varepsilon_{L_{22}} = \varepsilon_{L_3} = 0.1$, it gives

$$A_2 \leq \frac{2}{5} \sigma_r^* \|\Delta\|_F^2 \quad (28)$$

holds for probability at least $1 - 3n^{1-\beta} - n^{2-\beta}$ inside the attractive region, given C_β large enough. By combining (28) and (22), we can decide the upper bound on $\|\Delta\|_F$

$$\begin{aligned} \langle \hat{\nabla} f(\mathbf{P}), \Delta \rangle &\geq \langle \mathbb{E} \hat{\nabla} f(\mathbf{P}), \Delta \rangle - \frac{2}{5} \sigma_r^* \|\Delta\|_F^2 \\ &\geq \left(\frac{5}{4} \sigma_r^* - \frac{2}{5} \sigma_r^* - 4 \|\Delta\|_F^2 \right) \|\Delta\|_F^2 \stackrel{(i)}{\geq} \frac{1}{2} \sigma_r^* \|\Delta\|_F^2, \end{aligned} \quad (29)$$

where (i) from forcing $\|\Delta\|_F^2 \leq \frac{7}{80} \sigma_r^*$, concluding the proof. \square

C. Restricted Smoothness: (19b)

Notice that $\|\hat{\nabla} f(\mathbf{P})\|_F^2 = |\sup_{\|\mathbf{Z}\|_F=1} \langle \hat{\nabla} f(\mathbf{P}), \mathbf{Z} \rangle|^2$, and $A_3 := |\langle \hat{\nabla} f(\mathbf{P}), \mathbf{Z} \rangle|^2$ can be separated as in (23). Define $\mathbf{Z}_\Delta := \mathbf{Z}\Delta^T + \Delta\mathbf{Z}^T$, and $\mathbf{Z}_{P^*} = \mathbf{Z}\bar{\mathbf{P}}^{*T} + \bar{\mathbf{P}}^*\mathbf{Z}^T \in \mathbb{T}$, we have

$$\begin{aligned} A_3 &= \left| \left\langle \frac{1}{p} \mathcal{R}_\Omega (\Delta\bar{\mathbf{P}}^{*T} + \bar{\mathbf{P}}^* \Delta^T + \Delta\Delta^T), \mathbf{Z}_{P^*} + \mathbf{Z}_\Delta \right\rangle \right|^2 \\ &\leq \left| \left\langle \frac{1}{p} \mathcal{R}_\Omega (\Delta\bar{\mathbf{P}}^{*T} + \bar{\mathbf{P}}^* \Delta^T), \mathbf{Z}_{P^*} \right\rangle \right|^2 \\ &\quad + \left| \left\langle \frac{1}{p} \mathcal{R}_\Omega (\Delta\bar{\mathbf{P}}^{*T} + \bar{\mathbf{P}}^* \Delta^T), \mathbf{Z}_\Delta \right\rangle \right|^2 \\ &\quad + \left| \left\langle \frac{1}{p} \mathcal{R}_\Omega (\Delta\Delta^T), \mathbf{Z}_\Delta \right\rangle + \left\langle \frac{1}{p} \mathcal{R}_\Omega (\Delta\Delta^T), \mathbf{Z}_{P^*} \right\rangle \right|^2 \\ &:= |R_1 + R_2 + R_3 + R_4|^2 \\ &\leq |R_1| + |R_2| + |R_3| + |R_4|^2. \end{aligned} \quad (30)$$

Bound on R_1 , R_2 , and R_3 : The upper bounds on the first three terms are meanwhile straightforward, thus we process them quickly. When $p \gtrsim \frac{C_\beta \mu^2 r^2 \log n}{\varepsilon_{R_1}^2 n}$ and inside the RIC, since $\|\mathbf{Z}\|_F = 1$, we have

$$|R_1| = \left| \left\langle \left(\frac{1}{p} \mathcal{P}_\mathbb{T} \mathcal{R}_\Omega \mathcal{P}_\mathbb{T} - \mathcal{P}_\mathbb{T} \right) (\Delta\bar{\mathbf{P}}^{*T} + \bar{\mathbf{P}}^* \Delta^T), \mathbf{Z}_{P^*} \right\rangle \right|$$

$$\begin{aligned} &+ \left| \left\langle \Delta\bar{\mathbf{P}}^{*T} + \bar{\mathbf{P}}^* \Delta^T, \mathbf{Z}_{P^*} \right\rangle \right| \\ &\stackrel{(i)}{\leq} 4(1 + \varepsilon_{R_1}) \sigma_1^* \|\Delta\|_F \|\mathbf{Z}\|_F \leq \frac{22}{5} \sigma_1^* \|\Delta\|_F, \end{aligned} \quad (31)$$

$$\begin{aligned} |R_2| &= \left| \left\langle \left(\frac{1}{p} \mathcal{R}_\Omega - \mathcal{I} \right) (\Delta\bar{\mathbf{P}}^{*T} + \bar{\mathbf{P}}^* \Delta^T), \mathbf{Z}_\Delta \right\rangle \right| \\ &+ \left| \left\langle \Delta\bar{\mathbf{P}}^{*T} + \bar{\mathbf{P}}^* \Delta^T, \mathbf{Z}_\Delta \right\rangle \right| \\ &\stackrel{(ii)}{\leq} (6c_g \sqrt{\frac{n}{p}} \|\Delta\|_{2,\infty} \|\mathbf{P}^*\|_{2,\infty} + 4\sigma_1^{*1/2} \|\Delta\|_F) \|\Delta\|_F \|\mathbf{Z}\|_F \\ &\stackrel{(iii)}{\lesssim} \left(\sqrt{\frac{c_I \mu^2 r^2 \sigma_1^{*2}}{np}} + \frac{6}{5} \sigma_1^* \right) \|\Delta\|_F \leq \frac{7}{5} \sigma_1^* \|\Delta\|_F, \end{aligned} \quad (32)$$

$$\begin{aligned} |R_3| &= \left| \left\langle \left(\frac{1}{p} \mathcal{R}_\Omega - \mathcal{I} \right) (\Delta\Delta^T), \mathbf{Z}_\Delta \right\rangle + \langle \Delta\Delta^T, \mathbf{Z}_\Delta \rangle \right| \\ &\stackrel{(iv)}{\leq} (3c_g \sqrt{\frac{n}{p}} \|\Delta\|_{2,\infty}^2 + 2\|\Delta\|_F^2) \|\Delta\|_F \|\mathbf{Z}\|_F \\ &\stackrel{(v)}{\lesssim} \left(\sqrt{\frac{c_I^2 \mu^2 r^2 \sigma_1^{*2}}{np}} + \frac{7}{40} \sigma_1^* \right) \|\Delta\|_F \leq \frac{1}{5} \sigma_1^* \|\Delta\|_F, \end{aligned} \quad (33)$$

where (i) from Lemma C.3 and set $\varepsilon_{R_1} = 0.1$, (ii), (iv) from Lemma B.1, (iii), (v) by the assumption on \mathbf{P}^* and the RIC.

Bound on R_4 : This is the largest one since it does not follow from Lemma B.2. We are inclined to believe that it is hard to substantively improve the estimate below, i.e., to get rid of μ , r . Notice that w.l.o.g., we can assume $\mathbf{Z}^T \mathbf{1} = \mathbf{0}$ as $\mathbf{Z}_{P^*} \in \mathbb{T}$. Therefore $\mathbf{J}\mathbf{Z}_{P^*}\mathbf{J} = \mathbf{Z}_{P^*}$, it gives

$$\begin{aligned} |R_4| &= \left| \left\langle \frac{1}{p} g^+ \mathcal{P}_\Omega g (\Delta\Delta^T), \mathbf{Z}_{P^*} \right\rangle \right| \\ &= \left| \left\langle \frac{1}{p} \mathcal{P}_\Omega g (\Delta\Delta^T), \mathcal{P}_\Omega g^+ (\mathbf{Z}_{P^*}) \right\rangle \right| \\ &\stackrel{(i)}{\leq} \frac{1}{2} \sqrt{\frac{1}{p} \|\mathcal{Q}_\Omega (\Delta\Delta^T)\|_F^2} \sqrt{\frac{1}{p} \|\mathcal{P}_\Omega \mathcal{P}_\mathbb{T} (\mathbf{Z}_{P^*})\|_F^2} \\ &\stackrel{(ii)}{\leq} \frac{63\sigma_1^* \sqrt{c_I \mu r}}{20} \|\Delta\|_F, \end{aligned} \quad (34)$$

where (i) uses the structure of g^+ and followed by Cauchy-Schwarz. And (ii) dues to combining

$$\begin{aligned} &\frac{1}{p} \|\mathcal{Q}_\Omega (\Delta\Delta^T)\|_F^2 \\ &\stackrel{(a)}{\leq} (8c_I \mu r \sigma_1^* + \sqrt{\frac{c\beta c_I^2 \mu^2 r^2 \sigma_1^{*2} \log n}{np}} + \frac{7}{10} \sigma_r^*) \|\Delta\|_F^2 \\ &\stackrel{(b)}{\leq} 9c_I \mu r \sigma_1^* \|\Delta\|_F^2, \end{aligned}$$

and $\sqrt{\frac{1}{p} \|\mathcal{P}_\Omega \mathcal{P}_\mathbb{T} (\mathbf{Z}_{P^*})\|_F^2} \stackrel{(c)}{\leq} \sqrt{\frac{11}{10}} \|\mathbf{Z}_{P^*}\|_F \leq \frac{\sqrt{110}\sigma_1^*}{5} \|\mathbf{Z}\|_F$. Where (a) from Lemma C.5 and then use the RIC assumption on \mathcal{B} , (b) by forcing $p \gtrsim \frac{C_\beta \mu^2 r^2 \log n}{\varepsilon_{R_1}^2 n}$, and (c) from Lemma C.4 with $\varepsilon = 0.1$ and $p \gtrsim \frac{C_\beta \mu^2 r^2 \log n}{\varepsilon_{R_1}^2 n}$. We infer current bound on $\frac{1}{p} \|\mathcal{Q}_\Omega (\Delta\Delta^T)\|_F^2$, i.e., [22, Lemma B.2] or Lemma C.5, is not sharp up to \sqrt{n} , but we cannot amend it. If this estimate can be shown to be as good as the random graph lemma [33, Lemma 7.1], then one will immediately obtain the local convergence mechanism, i.e., the contraction speed measured by $\|\Delta\|_F$, when optimizing the s-stress function.

By substituting (31), (32), (33), and (34) into (30), it gives

$$\|\hat{\nabla} f(\mathbf{P})\|_F^2 \leq 84\sigma_1^{*2} c_I \mu r \|\Delta\|_F^2, \quad (35)$$

hold with probability at least $1 - cn^{1-\beta}$ in the RIC \mathcal{B} , provided with $p \gtrsim (C_\beta \mu^2 r^2 \log n)/n$ and C_β large enough, thus concluding the proof. \square

APPENDIX C SUPPORTING LEMMAS

Lemma C.1 ([74], Thm. 1.6). *If a finite sequence $\{\mathbf{S}_k\}$ of independent, random matrices of dimension $\mathbb{R}^{n_1 \times n_2}$ that satisfy*

$$\mathbb{E}\mathbf{S}_k = \mathbf{0}, \|\mathbf{S}_k\| \leq B \text{ almost surely.}$$

Let the norm of the total variance be

$$\sigma^2 := \max \left\{ \left\| \sum_k \mathbb{E}\mathbf{S}_k \mathbf{S}_k^T \right\|, \left\| \sum_k \mathbb{E}\mathbf{S}_k^T \mathbf{S}_k \right\| \right\}.$$

Then for all $t \geq 0$ we have

$$\mathbb{P} \left\{ \left\| \sum_k \mathbf{S}_k \right\| \geq t \right\} \leq (n_1 + n_2) \exp\left(\frac{-t^2}{2\sigma^2 + 2Bt/3}\right).$$

Lemma C.2 ([60], Coro. 3.12). *The random graph lemma, see also [33, Lemma 7.1]. If $p \geq \frac{C_g \beta \log n}{n}$ for some $C_g > 0$, $\beta > 1$,*

$$\left\| \frac{1}{p} \mathcal{P}_\Omega(\mathbf{H}_1) - \mathbf{H}_1 \right\| \leq c_g \sqrt{\frac{n}{p}},$$

holds with probability at least $1 - n^{1-\beta}$, where $\mathbf{H}_1 = \mathbf{1}\mathbf{1}^T - \mathbf{I}_n$.

Lemma C.3 ([23], Thm. 5.4). *The local Restricted Isometry Property (RIP) of \mathcal{R}_Ω . If $\|\mathbf{U}^*\|_{2,\infty}^2 \leq \frac{\mu r}{n}$, then for $\epsilon \geq \sqrt{\frac{C_r \beta (\mu r)^2 \log n}{np}}$*

$$\left\| \frac{1}{p} \mathcal{P}_\mathbb{T} \mathcal{R}_\Omega \mathcal{P}_\mathbb{T} - \mathcal{P}_\mathbb{T} \right\| \leq \epsilon < 1,$$

holds with probability at least $1 - n^{1-\beta}$ as soon as $p \geq C_r \beta (\mu r)^2 \log n/n$ for sufficient large constant C_r and $\beta > 1$.

Lemma C.4 ([38], Thm. 4.1). *The local RIP of \mathcal{P}_Ω . If $\|\mathbf{U}^*\|_{2,\infty}^2 \leq \frac{\mu r}{n}$, then for $\epsilon \geq \sqrt{\frac{C_r \beta \mu r \log n}{np}}$*

$$\left\| \frac{1}{p} \mathcal{P}_\mathbb{T} \mathcal{P}_\Omega \mathcal{P}_\mathbb{T} - \mathcal{P}_\mathbb{T} \right\| \leq \epsilon < 1,$$

holds with probability at least $1 - n^{1-\beta}$ as soon as $p \geq C_r \beta \mu r \log n/n$ for sufficient large constant C_r and $\beta > 1$.

Lemma C.5. *If $p > C \frac{\beta \log n}{n}$, then uniformly for all matrices $\Delta \in \mathbb{R}^{n \times r}$,*

$$\begin{aligned} & \frac{1}{p} \|\mathcal{Q}_\Omega(\Delta \Delta^T)\|_F^2 \\ & \leq \left[(8n + \sqrt{\frac{c\beta n \log n}{p}}) \|\Delta\|_{2,\infty}^2 + 8\|\Delta\|_F^2 \right] \|\Delta\|_F^2, \end{aligned}$$

holds with probability at least $1 - n^{1-\beta}$. This is in fact an unpublished result in the extended version of [22], but for completeness we reprove it here in App. D-C.

Lemma C.6 ([1], Thm. I.1). *See also [23, Lemma 5.6]. Under the set up of Theorem II.1, for some $0 < \epsilon \leq 1$, we have*

$$\left\| \mathcal{T}_r \left[-\frac{1}{2p} \mathbf{J}(\mathcal{P}_\Omega \mathbf{D}^*) \mathbf{J} \right] - \mathbf{G}^* \right\| \leq \epsilon \|\mathbf{G}^*\|, \quad (36)$$

holds with probability at least $1 - n^{1-\beta}$ as soon as $p \geq C_s \beta (\mu r)^2 \log n/(\epsilon^2 n)$.

Lemma C.7 ([34], Prop. B.4). *For any matrix $\mathbf{E} \in \mathbb{R}^{n \times r}$, $\mathbf{F} \in \mathbb{R}^{r \times n}$, $r \leq n$, we have*

$$\sigma_{\min}(\mathbf{E}) \|\mathbf{F}\|_F \leq \|\mathbf{E}\mathbf{F}\|_F \leq \|\mathbf{E}\| \|\mathbf{F}\|_F.$$

APPENDIX D PROOF OF AUXILIARY LEMMAS

The proof of Lemma B.1 and B.2 is partly inspired by [70, Lemma 8] [71, Lemma 22], and [61, Thm. 4.1], respectively.

A. Proof of Lemma B.1

Notice that

$$\left| \left\langle \left(\frac{1}{p} \mathcal{R}_\Omega - \mathcal{I} \right) (\mathbf{A}\mathbf{B}^T), \mathbf{C}\mathbf{D}^T \right\rangle \right| \leq \left\| \left(\frac{1}{p} \mathcal{R}_\Omega - \mathcal{I} \right) (\mathbf{A}\mathbf{B}^T) \right\| \|\mathbf{C}\mathbf{D}^T\|_F,$$

and

$$\begin{aligned} \left\| \left(\frac{1}{p} \mathcal{R}_\Omega - \mathcal{I} \right) (\mathbf{A}\mathbf{B}^T) \right\| &= \left\| \frac{1}{p} g^+ \mathcal{P}_\Omega g(\mathbf{A}\mathbf{B}^T) - g^+ g(\mathbf{A}\mathbf{B}^T) \right\| \\ &= \frac{1}{2} \|\mathbf{J}\| \left\| \frac{1}{p} \mathcal{P}_\Omega g(\mathbf{A}\mathbf{B}^T) - g(\mathbf{A}\mathbf{B}^T) \right\| \|\mathbf{J}\| \\ &\leq \frac{1}{2} \left\| \frac{1}{p} \mathcal{P}_\Omega g(\mathbf{A}\mathbf{B}^T) - g(\mathbf{A}\mathbf{B}^T) \right\| = \frac{1}{2} I_1. \end{aligned}$$

Using the variational characterization of spectral norm, we have

$$\begin{aligned} I_1 &:= \sup_{\mathbf{x}, \mathbf{y} \in \mathbb{S}^{n-1}} \left\langle \frac{1}{p} \mathcal{P}_\Omega g(\mathbf{A}\mathbf{B}^T) - g(\mathbf{A}\mathbf{B}^T), \mathbf{x}\mathbf{y}^T \right\rangle \\ &\stackrel{(i)}{=} \sup_{\mathbf{x}, \mathbf{y} \in \mathbb{S}^{n-1}} \left\langle \frac{1}{p} \mathcal{P}_\Omega(\mathbf{H}_1) - \mathbf{H}_1, g(\mathbf{A}\mathbf{B}^T) \circ \mathbf{x}\mathbf{y}^T \right\rangle \\ &\leq \left\| \frac{1}{p} \mathcal{P}_\Omega(\mathbf{H}_1) - \mathbf{H}_1 \right\| \sup_{\mathbf{x}, \mathbf{y} \in \mathbb{S}^{n-1}} \|g(\mathbf{A}\mathbf{B}^T) \circ \mathbf{x}\mathbf{y}^T\|_* \\ &\stackrel{(ii)}{\leq} c_g \sqrt{\frac{n}{p}} \sup_{\mathbf{x}, \mathbf{y} \in \mathbb{S}^{n-1}} I_2(\mathbf{x}, \mathbf{y}), \end{aligned}$$

where (i) by noticing

$$\frac{1}{p} \mathcal{P}_\Omega g(\mathbf{A}\mathbf{B}^T) - g(\mathbf{A}\mathbf{B}^T) = \left(\frac{1}{p} \mathcal{P}_\Omega(\mathbf{H}_1) - \mathbf{H}_1 \right) \circ g(\mathbf{A}\mathbf{B}^T)$$

and then using the identity $\text{tr}(\mathbf{A}^T(\mathbf{B} \circ \mathbf{C})) = \text{tr}((\mathbf{A}^T \circ \mathbf{B}^T)\mathbf{C})$, and (ii) from Lemma C.2. By (7) and triangle inequality, I_2 reduces to

$$\begin{aligned} I_2 &\leq \|\text{diag}(\mathbf{A}\mathbf{B}^T) \mathbf{1}^T \circ \mathbf{x}\mathbf{y}^T\|_* + \|\mathbf{1} \text{diag}(\mathbf{A}\mathbf{B}^T)^T \circ \mathbf{x}\mathbf{y}^T\|_* \\ &\quad + 2\|\mathbf{A}\mathbf{B}^T \circ \mathbf{x}\mathbf{y}^T\|_* = I_{21} + I_{22} + 2I_{23}. \end{aligned}$$

For I_{21} and I_{22} , recall $\mathbf{A} = [\mathbf{A}_{1,\cdot}, \dots, \mathbf{A}_{n,\cdot}]^T$, $\mathbf{B} = [\mathbf{B}_{1,\cdot}, \dots, \mathbf{B}_{n,\cdot}]^T$. By the identity $(\mathbf{a}\mathbf{b}^T) \circ (\mathbf{c}\mathbf{d}^T) = (\mathbf{a} \circ \mathbf{c})(\mathbf{b} \circ \mathbf{d})^T$, we have

$$\begin{aligned} I_{21} &= \|(\text{diag}(\mathbf{A}\mathbf{B}^T) \circ \mathbf{x})(\mathbf{1} \circ \mathbf{y})^T\|_* \\ &\leq \left\| \begin{bmatrix} \mathbf{x}_1 \mathbf{A}_{1,\cdot}^T \mathbf{B}_{1,\cdot} \\ \vdots \\ \mathbf{x}_n \mathbf{A}_{n,\cdot}^T \mathbf{B}_{n,\cdot} \end{bmatrix} \right\|_2 \|\mathbf{y}\|_2 \leq \sqrt{\sum_{i=1}^n \mathbf{x}_i^2 (\mathbf{A}_{i,\cdot}^T \mathbf{B}_{i,\cdot})^2} \end{aligned}$$

$$\leq \max_{i \in [n]} \|\mathbf{A}_{i,\cdot}^T \mathbf{B}_{i,\cdot}\| \cdot \|\mathbf{x}\|_2 \leq \|\mathbf{A}\mathbf{B}^T\|_\infty.$$

Same bound holds for I_{22} . By [69, Lemma 5], I_{23} can be decomposed as

$$\begin{aligned} I_{23} &= \left\| \left(\sum_{k=1}^r \mathbf{A}_{\cdot,k} \mathbf{B}_{\cdot,k}^T \right) \circ \mathbf{xy}^T \right\|_* = \left\| \sum_{k=1}^r (\mathbf{A}_{\cdot,k} \circ \mathbf{x})(\mathbf{B}_{\cdot,k} \circ \mathbf{y})^T \right\|_* \\ &\leq \sum_{k=1}^r \|(\mathbf{A}_{\cdot,k} \circ \mathbf{x})(\mathbf{B}_{\cdot,k} \circ \mathbf{y})^T\|_* \leq \sum_{k=1}^r \|\mathbf{A}_{\cdot,k} \circ \mathbf{x}\|_2 \|\mathbf{B}_{\cdot,k} \circ \mathbf{y}\|_2 \\ &\stackrel{(i)}{\leq} \sqrt{\sum_{i=1}^n \mathbf{x}_i^2 \sum_{k_1=1}^r \mathbf{A}_{ik_1}^2} \sqrt{\sum_{j=1}^n \mathbf{y}_j^2 \sum_{k_2=1}^r \mathbf{B}_{jk_2}^2} \\ &\leq \|\mathbf{A}\|_{2,\infty} \|\mathbf{B}\|_{2,\infty}, \end{aligned} \quad (37)$$

where (i) from Cauchy-Schwarz. Since $\|\mathbf{A}\mathbf{B}^T\|_\infty \leq \|\mathbf{A}\|_{2,\infty} \|\mathbf{B}\|_{2,\infty}$, we have

$$\left\| \left(\frac{1}{p} \mathcal{R}_\Omega - \mathcal{I} \right) (\mathbf{A}\mathbf{B}^T) \right\| \leq 2c_g \sqrt{\frac{n}{p}} \|\mathbf{A}\|_{2,\infty} \|\mathbf{B}\|_{2,\infty},$$

holds uniformly over all $\mathbf{A}, \mathbf{B} \in \mathbb{R}^{n \times r}$ with probability at least $1 - n^{1-\beta}$ given $p \gtrsim \frac{\beta \log n}{n}$, concluding the proof. \square

B. Proof of Lemma B.2

Unfortunately, same strategy as in App. D-A does not apply to Lemma B.2, due to the asymmetry structure of \mathcal{R}_Ω . Uniform bound presents here largely dues to the fixed, incoherent matrix \mathbf{B} . Let $\mathbf{X} = \mathbf{A}\mathbf{R}^T\mathbf{B}^T$, we need to control $T_0 = \|(\frac{1}{p}\mathcal{R}_\Omega^* - \mathcal{I})\mathbf{X}\|$, where $\mathbf{X} = \mathbf{J}\mathbf{X}\mathbf{J}$ always holds. Notice that by using the structure of $g^*(\mathbf{D}) := 2(\text{diag}(\mathbf{D}\mathbf{1}) - \mathbf{D})$, T_0 can be reduced to

$$\begin{aligned} T_0 &= \left\| \frac{-1}{2p} g^* \mathcal{P}_\Omega \mathbf{X} - \mathbf{X} \right\| \\ &= \left\| \frac{1}{p} \text{diag}((\mathcal{P}_\Omega \mathbf{X})\mathbf{1}) + \frac{1}{p} \mathcal{P}_\Omega \mathbf{X} - \mathbf{X} \right\| \\ &\stackrel{(i)}{\leq} \left\| \left(\frac{1}{p} \mathcal{P}_\Omega \mathbf{X} \right) \mathbf{1} - \text{diag}(\mathbf{X}) \right\|_\infty + \left\| \frac{1}{p} \mathcal{P}_\Omega \mathbf{X} - \text{Od}(\mathbf{X}) \right\| \\ &\stackrel{(ii)}{\leq} \underbrace{\left\| \left(\frac{1}{p} \mathcal{P}_\Omega \mathbf{X} - \text{Od}(\mathbf{X}) \right) \mathbf{1} \right\|_\infty}_{T_1} + \underbrace{\left\| \frac{1}{p} \mathcal{P}_\Omega \mathbf{X} - \text{Od}(\mathbf{X}) \right\|}_{T_2} \end{aligned}$$

where (i) use the fact that Ω is a hollow diagonal sample set, and (ii) by noticing $\mathbf{X}\mathbf{1} = \mathbf{0}$, i.e., $\mathbf{e}_i^T \text{Od}(\mathbf{X})\mathbf{1} = \sum_{j \neq i} \mathbf{X}_{ij} = \mathbf{X}_{ii}$ for $i \in [n]$.

Bound on T_2 : This follows from similar argument as in [71, Lemma 22], thus holds uniformly over \mathbf{A}, \mathbf{B} , and \mathbf{R} . By using the same trick as in App. D-A, one can show

$$\begin{aligned} T_2 &= \sup_{\mathbf{x}, \mathbf{y} \in \mathcal{S}^{n-1}} \left\langle \frac{1}{p} \mathcal{P}_\Omega(\mathbf{H}\mathbf{1}) - \mathbf{H}\mathbf{1}, \text{Od}(\mathbf{A}\bar{\mathbf{B}}^T) \circ \mathbf{xy}^T \right\rangle \\ &\leq c_g \sqrt{\frac{n}{p}} \left\| \text{Od}(\mathbf{A}\bar{\mathbf{B}}^T) \circ \mathbf{xy}^T \right\|_* = c_g \sqrt{\frac{n}{p}} T_3. \end{aligned} \quad (38)$$

where we set $\bar{\mathbf{B}} = \mathbf{B}\mathbf{R}$ for any $\mathbf{R} \in O(r)$. By subtracting and adding terms, it gives

$$T_3 \leq \underbrace{\|\mathbf{A}\bar{\mathbf{B}}^T \circ \mathbf{xy}^T\|_*}_{T_{31}} + \underbrace{\|(\mathbf{I} \circ \mathbf{A}\bar{\mathbf{B}}^T) \circ \mathbf{xy}^T\|_*}_{T_{32}},$$

and the same upper bound in (37) applies to T_{31} . For T_{32} , first recall the column blocking structure, we have

$$\begin{aligned} (\mathbf{I} \circ \mathbf{A}\bar{\mathbf{B}}^T) \circ \mathbf{xy}^T &= \sum_{i=1}^n \left\langle \sum_{k=1}^r \mathbf{A}_{\cdot,k} \bar{\mathbf{B}}_{\cdot,k}^T, (\mathbf{e}_i \mathbf{e}_i^T) \circ \mathbf{xy}^T \right\rangle \mathbf{e}_i \mathbf{e}_i^T \\ &= \sum_{i=1}^n \left\langle \sum_{k=1}^r \mathbf{A}_{ik} \bar{\mathbf{B}}_{ik} \mathbf{x}_i \mathbf{y}_i \right\rangle \mathbf{e}_i \mathbf{e}_i^T. \end{aligned}$$

Next, by using the identity $\|\mathbf{Y}\|_* = \text{tr}(\sqrt{\mathbf{Y}^T \mathbf{Y}})$, it gives

$$\begin{aligned} T_{32} &= \sum_{i=1}^n \sqrt{\left(\sum_{k=1}^r \mathbf{A}_{ik} \mathbf{x}_i \bar{\mathbf{B}}_{ik} \mathbf{y}_i \right)^2} \\ &\stackrel{(i)}{\leq} \sum_{i=1}^n \sqrt{\left(\sum_{k_1=1}^r \mathbf{A}_{ik_1}^2 \mathbf{x}_i^2 \right) \left(\sum_{k_2=1}^r \bar{\mathbf{B}}_{ik_2}^2 \mathbf{y}_i^2 \right)} \\ &\stackrel{(ii)}{\leq} \sqrt{\sum_{i=1}^n \sum_{k_1=1}^r \mathbf{A}_{ik_1}^2 \mathbf{x}_i^2} \sqrt{\sum_{j=1}^n \sum_{k_2=1}^r \bar{\mathbf{B}}_{jk_2}^2 \mathbf{y}_j^2} \\ &\stackrel{(iii)}{\leq} \|\mathbf{A}\|_{2,\infty} \|\mathbf{B}\|_{2,\infty}, \end{aligned} \quad (39)$$

where (i), (ii) use Cauchy-Schwarz, (iii) from same argument as in (37). Thus $T_3 \leq 2\|\mathbf{A}\|_{2,\infty} \|\mathbf{B}\|_{2,\infty}$. By substituting (39) into (38), we conclude the first part of the proof.

Bound on T_1 : The uniform result does not apply to \mathbf{B} , yet the orthogonal matrix \mathbf{R} can be automatically canceled out after some transformation, thus eliminating a covering argument over $O(r)$. W.l.o.g. we can introduce diagonal samples, i.e., let $\{\delta_{ii}\}_{i=1}^n$ be the i.i.d. copy of δ_{ij} . Assume for the moment that $\tilde{\Omega} = \Omega \cup \{\delta_{ii}\}_{i=1}^n$, by adding and subtracting terms, we have

$$\begin{aligned} T_1 &\leq \left\| \left(\frac{1}{p} \mathcal{P}_{\tilde{\Omega}} \mathbf{X} - \mathbf{X} \right) \mathbf{1} \right\|_\infty + \left\| \text{diag} \left(\frac{1}{p} \mathcal{P}_{\tilde{\Omega}} \mathbf{X} - \mathbf{X} \right) \right\|_\infty \\ &\leq \left\| \left(\frac{1}{p} \mathcal{P}_{\tilde{\Omega}} \mathbf{X} \right) \mathbf{1} \right\|_\infty + \frac{1}{p} \|\mathbf{X}\|_\infty \\ &= \max_{m \in [n]} \left| \left\langle \frac{1}{p} \mathcal{P}_{\tilde{\Omega}}(\mathbf{1}\mathbf{1}^T), \mathbf{A}\bar{\mathbf{B}}^T \circ \mathbf{e}_m \mathbf{1}^T \right\rangle \right| + \frac{1}{p} \|\mathbf{X}\|_\infty. \end{aligned}$$

We first separate \mathbf{A} in T_{11} , inspired by the following trick [61, Thm. 4.1]

$$\begin{aligned} T_{11} &= \left\langle \frac{1}{p} \mathcal{P}_{\tilde{\Omega}}(\mathbf{1}\mathbf{1}^T), \sum_{k=1}^r (\mathbf{A}_{\cdot,k} \bar{\mathbf{B}}_{\cdot,k}^T) \circ \mathbf{e}_m \mathbf{1}^T \right\rangle \\ &= \sum_{k=1}^r (\mathbf{A}_{\cdot,k} \circ \mathbf{e}_m)^T \frac{1}{p} \mathcal{P}_{\tilde{\Omega}}(\mathbf{1}\mathbf{1}^T) \bar{\mathbf{B}}_{\cdot,k} \\ &\stackrel{(i)}{\leq} \sqrt{\sum_{k=1}^r \mathbf{A}_{mk}^2} \sqrt{\sum_{k=1}^r \left| \mathbf{e}_m^T \frac{1}{p} \mathcal{P}_{\tilde{\Omega}}(\mathbf{1}\mathbf{1}^T) \bar{\mathbf{B}}_{\cdot,k} \right|^2} \\ &\leq \|\mathbf{A}\|_{2,\infty} \sqrt{\sum_{k=1}^r \left| \mathbf{e}_m^T \left(\frac{1}{p} \mathcal{P}_{\tilde{\Omega}}(\mathbf{1}\mathbf{1}^T) - \mathbf{1}\mathbf{1}^T \right) \bar{\mathbf{B}}_{\cdot,k} \right|^2}, \end{aligned} \quad (40)$$

where (i) from Cauchy-Schwarz. Set $\mathbf{G} = \frac{1}{p}\mathcal{P}_{\Omega}(\mathbf{1}\mathbf{1}^T) - \mathbf{1}\mathbf{1}^T$ for the moment, notice that

$$\begin{aligned}\bar{T}_{11} &= \sqrt{\mathbf{e}_m^T \mathbf{G} \sum_{k=1}^r (\bar{\mathbf{B}}_{\cdot,k} \bar{\mathbf{B}}_{\cdot,k}^T) \mathbf{G}^T \mathbf{e}_m} \\ &= \sqrt{\mathbf{e}_m^T \mathbf{G} \bar{\mathbf{B}} \bar{\mathbf{B}}^T \mathbf{G}^T \mathbf{e}_m} = \|\mathbf{e}_m^T \mathbf{G} \mathbf{B} \mathbf{R}\|_2 \\ &= \left\| \sum_{j=1}^n \left(\frac{1}{p} \delta_{mj} - 1 \right) \mathbf{B}_{j,\cdot}^T \right\|_2 = \left\| \sum_{j=1}^n \mathbf{S}_{mj} \right\|_2,\end{aligned}$$

holds for all $\mathbf{R} \in O(r)$. It is then straightforward to check

$$\mathbb{E} \mathbf{S}_{mj} = \mathbf{0}, \|\mathbf{S}_{mj}\|_2 \leq \frac{1}{p} \|\mathbf{B}\|_{2,\infty},$$

and

$$\begin{aligned}\left\| \sum_{j=1}^n \mathbb{E} \mathbf{S}_{mj}^T \mathbf{S}_{mj} \right\| &\leq \frac{1}{p} \left\| \sum_{j=1}^n \mathbf{B}_{j,\cdot} \mathbf{B}_{j,\cdot}^T \right\| = \frac{1}{p} \|\mathbf{B}^T \mathbf{B}\| \leq \frac{1}{p} \|\mathbf{B}\|^2, \\ \left| \sum_{j=1}^n \mathbb{E} \mathbf{S}_{mj} \mathbf{S}_{mj}^T \right| &\leq \frac{1}{p} \left| \sum_{j=1}^n \mathbf{B}_{j,\cdot}^T \mathbf{B}_{j,\cdot} \right| \leq \frac{n}{p} \|\mathbf{B}\|_{2,\infty}^2.\end{aligned}$$

Using elementary bound $\|\mathbf{B}\|^2 \leq \|\mathbf{B}\|_F^2 \leq n \|\mathbf{B}\|_{2,\infty}^2$ and Lemma C.1, we have

$$\begin{aligned}\bar{T}_{11} &\leq \frac{C\beta \log n \|\mathbf{B}\|_{2,\infty}}{p} + \sqrt{\frac{C\beta n \log n \|\mathbf{B}\|_{2,\infty}^2}{p}} \\ &\leq \sqrt{\frac{C\beta n \log n}{p}} \|\mathbf{B}\|_{2,\infty},\end{aligned}\quad (41)$$

holds with probability at least $1 - n^{1-\beta}$ provided with $p \geq C\beta \log n/n$. By substituting (41) into (40), it gives

$$T_{11} \leq \sqrt{\frac{C\beta n \log n}{p}} \|\mathbf{A}\|_{2,\infty} \|\mathbf{B}\|_{2,\infty}.$$

Whenever $p \geq 1/n$, T_{11} dominates T_{12} , after a union bound over $m \in [n]$, we conclude the whole proof. \square

C. Proof of Lemma C.5

The original proof [75, App. B-D] has some flaws, but we have amended it here. Notice that by (12) and Cauchy-Schwarz, we have

$$\begin{aligned}\frac{1}{p} \|\mathcal{Q}_{\Omega} \Delta \Delta^T\|_F^2 &= \sum_{\alpha \in \mathbb{I}} \frac{2}{p} \delta_{\alpha} \langle \Delta \Delta^T, \boldsymbol{\omega}_{\alpha} \rangle^2 \\ &\leq \sum_{\alpha \in \mathbb{I}} \frac{8}{p} \delta_{\alpha} (\|\mathbf{e}_i^T \Delta\|_2^4 + \|\mathbf{e}_j^T \Delta\|_2^4 + 2\|\mathbf{e}_i^T \Delta\|_2^2 \|\mathbf{e}_j^T \Delta\|_2^2) \\ &= 8 \left\langle \sum_{\alpha \in \mathbb{I}} \frac{1}{p} \delta_{\alpha} \boldsymbol{\omega}_{\alpha+}, \mathbf{x} \mathbf{x}^T \right\rangle \\ &\leq 8 \left\langle \sum_{\alpha \in \mathbb{I}} \left(\frac{1}{p} \delta_{\alpha} - 1 \right) \boldsymbol{\omega}_{\alpha+}, \mathbf{x} \mathbf{x}^T \right\rangle + 8 \mathbf{x}^T (n \mathbf{I} + \mathbf{1} \mathbf{1}^T) \mathbf{x} \\ &\leq 8 \left\langle \sum_{\alpha \in \mathbb{I}} \mathbf{B}_{\alpha}, \mathbf{x} \mathbf{x}^T \right\rangle + 8n \|\mathbf{x}\|_2^2 + 8 \|\mathbf{x}\|_1^2 \\ &\leq (8 \left\| \sum_{\alpha \in \mathbb{I}} \mathbf{B}_{\alpha} \right\| + 8n) \|\mathbf{x}\|_2^2 + 8 \|\mathbf{x}\|_1^2\end{aligned}\quad (42)$$

where we set $\mathbf{x} = [\|\mathbf{e}_1^T \Delta\|_2^2, \dots, \|\mathbf{e}_n^T \Delta\|_2^2]^T$, $\boldsymbol{\omega}_{\alpha+} = |\boldsymbol{\omega}_{\alpha}| = (\mathbf{e}_i + \mathbf{e}_j)(\mathbf{e}_i + \mathbf{e}_j)^T$, and $\sum_{\alpha \in \mathbb{I}} \boldsymbol{\omega}_{\alpha+} = (n-2)\mathbf{I} + \mathbf{1}\mathbf{1}^T$. It remains to control the spectral norm of $\sum_{\alpha \in \mathbb{I}} (\frac{1}{p} \delta_{\alpha} - 1) \boldsymbol{\omega}_{\alpha+} := \sum_{\alpha \in \mathbb{I}} \mathbf{B}_{\alpha}$. It is straightforward to show

$$\mathbb{E} \mathbf{B}_{\alpha} = \mathbf{0}, \|\mathbf{B}_{\alpha}\| \leq \frac{1}{p} \|\boldsymbol{\omega}_{\alpha+}\| \leq \frac{2}{p},$$

and

$$\begin{aligned}\left\| \mathbb{E} \sum_{\alpha \in \mathbb{I}} \mathbf{B}_{\alpha}^2 \right\| &\leq \frac{1}{p} \left\| \sum_{\alpha \in \mathbb{I}} \boldsymbol{\omega}_{\alpha+}^2 \right\| \leq \frac{4}{p} \left\| \sum_{\alpha \in \mathbb{I}} \boldsymbol{\omega}_{\alpha+} \right\| \\ &\leq \frac{4}{p} \|n \mathbf{I} + \mathbf{1} \mathbf{1}^T\| \leq \frac{8n}{p},\end{aligned}$$

since $\boldsymbol{\omega}_{\alpha+}^2 \preceq 4\boldsymbol{\omega}_{\alpha+}$, $\forall \alpha \in \mathbb{I}$. From Lemma C.1, we have

$$\left\| \sum_{\alpha \in \mathbb{I}} \left(\frac{1}{p} \delta_{\alpha} - 1 \right) \boldsymbol{\omega}_{\alpha+} \right\| \leq \sqrt{\frac{c\beta n \log n}{p}},\quad (43)$$

holds with probability at least $1 - n^{1-\beta}$ given $p \geq C\beta \log n/n$. By substituting (43) into (42), it gives

$$\begin{aligned}\frac{1}{p} \|\mathcal{Q}_{\Omega} \Delta \Delta^T\|_F^2 &\leq \left(\sqrt{\frac{c\beta n \log n}{p}} + 8n \right) \|\mathbf{x}\|_2^2 + 8 \|\mathbf{x}\|_1^2 \\ &\leq \left[\left(\sqrt{\frac{c\beta n \log n}{p}} + 8n \right) \|\Delta\|_{2,\infty}^2 + 8 \|\Delta\|_F^2 \right] \|\Delta\|_F^2,\end{aligned}$$

holds for any Δ , thus concluding the proof. \square

REFERENCES

- [1] Y. Li and X. Sun, "One-step spectral estimation for euclidean distance matrix approximation," in *Asia Pac. Signal Inf. Process. Assoc. Annu. Summit Conf.*, 2024, pp. 1–6.
- [2] L. Van Der Maaten, E. Postma, and J. Van den Herik, "Dimensionality reduction: a comparative review," *J. Mach. Learn. Res.*, vol. 10, no. 66-71, p. 13, 2009.
- [3] N. Saeed, H. Nam, T. Y. Al-Naffouri, and M.-S. Alouini, "A state-of-the-art survey on multidimensional scaling-based localization techniques," *IEEE Commun. Surv. Tutorials*, vol. 21, no. 4, pp. 3565–3583, 2019.
- [4] I. Dokmanic, R. Parhizkar, J. Ranieri, and M. Vetterli, "Euclidean distance matrices: Essential theory, algorithms, and applications," *IEEE Signal Process. Mag.*, vol. 32, no. 6, pp. 12–30, 2015.
- [5] L. Liberti, C. Lavor, N. Maculan, and A. Mucherino, "Euclidean distance geometry and applications," *SIAM Rev.*, vol. 56, no. 1, pp. 3–69, 2014.
- [6] G. M. Crippen, "Conformational analysis by energy embedding," *J. Comput. Chem.*, vol. 3, no. 4, pp. 471–476, 1982. [Online]. Available: <https://doi.org/10.1002/jcc.540030404>
- [7] B. Hendrickson, "The molecule problem: Exploiting structure in global optimization," *SIAM J. Optim.*, vol. 5, pp. 835–857, 1995.
- [8] M. Cucuringu, A. Singer, and D. Curburn, "Eigenvector synchronization, graph rigidity and the molecule problem," *Inf. Inference J. IMA*, vol. 1, no. 1, pp. 21–67, 2012.
- [9] N.-H. Z. Leung and K.-C. Toh, "An sdp-based divide-and-conquer algorithm for large-scale noisy anchor-free graph realization," *SIAM J. Sci. Comput.*, vol. 31, no. 6, pp. 4351–4372, 2010.
- [10] P. Biswas, T.-C. Lian, T.-C. Wang, and Y. Ye, "Semidefinite programming based algorithms for sensor network localization," *ACM Trans. Sen. Netw.*, vol. 2, no. 2, p. 188–220, 2006.
- [11] P. Biswas, T. C. Liang, K. C. Toh, Y. Ye, and T. C. Wang, "Semidefinite programming approaches for sensor network localization with noisy distance measurements," *IEEE Trans. Autom. Sci. Eng.*, vol. 3, no. 4, pp. 360–371, 2006.
- [12] A. Javanmard and A. Montanari, "Localization from incomplete noisy distance measurements," *Found. Comput. Math.*, vol. 13, no. 3, pp. 297–345, 2013.
- [13] F. Marić, M. Giamou, A. W. Hall, S. Khoubyarian, I. Petrović, and J. Kelly, "Riemannian optimization for distance-geometric inverse kinematics," *IEEE Trans. Robot.*, vol. 38, no. 3, pp. 1703–1722, 2022.
- [14] P. Agostini, Z. Utkovski, and S. Stańczak, "Channel Charting: an Euclidean distance matrix completion perspective," in *Proc. Int. Conf. Acoust. Speech Signal Process.*, 2020, pp. 5010–5014.

- [15] P. Tabaghi, I. Dokmanić, and M. Vetterli, “Kinetic Euclidean distance matrices,” *IEEE Trans. Signal Process.*, vol. 68, pp. 452–465, 2020.
- [16] R. Parhizkar, A. Karbasi, S. Oh, and M. Vetterli, “Calibration using matrix completion with application to ultrasound tomography,” *IEEE Trans. Signal Process.*, vol. 61, no. 20, pp. 4923–4933, 2013.
- [17] L. Liberti, “Distance geometry and data science,” *TOP*, vol. 28, no. 2, pp. 271–339, 2020.
- [18] F. J. Király, L. Theran, and R. Tomioka, “The algebraic combinatorial approach for low-rank matrix completion,” *J. Mach. Learn. Res.*, vol. 16, no. 1, pp. 1391–1436, 2015.
- [19] A. Shapiro, Y. Xie, and R. Zhang, “Matrix completion with deterministic pattern: A geometric perspective,” *IEEE Trans. Signal Process.*, vol. 67, no. 4, pp. 1088–1103, 2019.
- [20] A. Tasissa and R. Lai, “Exact reconstruction of Euclidean distance geometry problem using low-rank matrix completion,” *IEEE Trans. Inf. Theory*, vol. 65, no. 5, pp. 3124–3144, 2019.
- [21] F. J. Király and L. Theran, “Coherence and sufficient sampling densities for reconstruction in compressed sensing,” *arXiv preprint arXiv:1302.2767*, 2013.
- [22] Y. Li and X. Sun, “Sensor network localization via riemannian conjugate gradient and rank reduction,” *IEEE Trans. Signal Process.*, vol. 72, pp. 1910–1927, 2024.
- [23] C. Smith, H. Cai, and A. Tasissa, “Riemannian optimization for non-convex euclidean distance geometry with global recovery guarantees,” *arXiv preprint arXiv:2410.06376*, 2024.
- [24] S. Oh, A. Montanari, and A. Karbasi, “Sensor network localization from local connectivity: Performance analysis for the MDS-MAP algorithm,” in *IEEE Inf. Theory Workshop*, 2010, pp. 1–5.
- [25] A. Montanari and S. Oh, “On positioning via distributed matrix completion,” in *IEEE Sens. Array Multichannel Signal Process. Workshop*, 2010, pp. 197–200.
- [26] A. Karbasi and S. Oh, “Robust localization from incomplete local information,” *IEEE/ACM Trans. Networking*, vol. 21, pp. 1131–1144, 2011.
- [27] A. M.-C. So and Y. Ye, “Theory of semidefinite programming for sensor network localization,” *Math. Program.*, vol. 109, no. 2-3, pp. 367–384, 2006.
- [28] J. Aspnes, T. Eren *et al.*, “A theory of network localization,” *IEEE Trans. Mob. Comput.*, vol. 5, no. 12, pp. 1663–1678, 2006.
- [29] Z. Zhu, A. M. C. So, and Y. Ye, “Universal rigidity: Towards accurate and efficient localization of wireless networks,” in *Proc. IEEE INFOCOM*, 2010, pp. 1–9.
- [30] A. M.-C. So and Y. Ye, “A semidefinite programming approach to tensegrity theory and realizability of graphs,” in *Proc. Annu. ACM SIAM Symp. Discrete Algorithms*, 2006, p. 766–775.
- [31] I. Ghosh, A. Tasissa, and C. Kümmerle, “Sample-efficient geometry reconstruction from euclidean distances using non-convex optimization,” *arXiv preprint arXiv:2410.16982*, 2024.
- [32] Y. Chen, “Incoherence-optimal matrix completion,” *IEEE Trans. Inf. Theory*, vol. 61, no. 5, pp. 2909–2923, 2015.
- [33] R. H. Keshavan, A. Montanari, and S. Oh, “Matrix completion from a few entries,” *IEEE Trans. Inf. Theory*, vol. 56, no. 6, pp. 2980–2998, 2010.
- [34] R. Sun and Z. Q. Luo, “Guaranteed matrix completion via non-convex factorization,” *IEEE Trans. Inf. Theory*, vol. 62, no. 11, pp. 6535–6579, 2016.
- [35] Q. Zheng and J. Lafferty, “Convergence analysis for rectangular matrix completion using Burer-Monteiro factorization and gradient descent,” *arXiv preprint arXiv:1605.07051*, 2016.
- [36] Y. Chen and M. J. Wainwright, “Fast low-rank estimation by projected gradient descent: General statistical and algorithmic guarantees,” *ArXiv*, vol. abs/1509.03025, 2015.
- [37] Y. Shang, W. Ruml, Y. Zhang, and M. P. J. Fromherz, “Localization from mere connectivity,” in *Proc. ACM Int. Symp. Mobile Ad hoc Netw. Comput.*, 2003, p. 201–212.
- [38] E. J. Candès and B. Recht, “Exact matrix completion via convex optimization,” *Found. Comput. Math.*, vol. 9, no. 6, pp. 717–772, 2009.
- [39] B. Recht, M. Fazel, and P. A. Parrilo, “Guaranteed minimum-rank solutions of linear matrix equations via nuclear norm minimization,” *SIAM Rev.*, vol. 52, no. 3, pp. 471–501, 2010.
- [40] D. Gross, “Recovering low-rank matrices from few coefficients in any basis,” *IEEE Trans. Inf. Theory*, vol. 57, no. 3, pp. 1548–1566, 2011.
- [41] A. Tasissa and R. Lai, “Low-rank matrix completion in a general non-orthogonal basis,” *Linear Algebra Appl.*, vol. 625, pp. 81–112, 2021.
- [42] S. Lichtenberg and A. Tasissa, “A dual basis approach to multidimensional scaling,” *Linear Algebra Appl.*, vol. 682, pp. 86–95, 2024.
- [43] E. J. Candès, X. Li, and M. Soltanolkotabi, “Phase retrieval via Wirtinger flow: Theory and algorithms,” *IEEE Trans. Inf. Theory*, vol. 61, no. 4, pp. 1985–2007, 2015.
- [44] J.-F. Cai, T. Wang, and K. Wei, “Spectral compressed sensing via projected gradient descent,” *SIAM J. Optim.*, vol. 28, no. 3, pp. 2625–2653, 2018.
- [45] J. Li, W. Cui, and X. Zhang, “Projected gradient descent for spectral compressed sensing via symmetric hankel factorization,” *IEEE Trans. Signal Process.*, vol. 72, pp. 1590–1606, 2024.
- [46] C. Ma, K. Wang, Y. Chi, and Y. Chen, “Implicit regularization in nonconvex statistical estimation: Gradient descent converges linearly for phase retrieval, matrix completion, and blind deconvolution,” *Found. Comput. Math.*, vol. 20, no. 3, pp. 451–632, 2020.
- [47] J. Chen, D. Liu, and X. Li, “Nonconvex rectangular matrix completion via gradient descent without $l_{2,\infty}$ regularization,” *IEEE Trans. Inf. Theory*, vol. 66, no. 9, pp. 5806–5841, 2020.
- [48] Y. Takane, F. W. Young, and J. de Leeuw, “Nonmetric individual differences multidimensional scaling: An alternating least squares method with optimal scaling features,” *Psychometrika*, vol. 42, no. 1, pp. 7–67, 1977. [Online]. Available: <https://doi.org/10.1007/BF02293745>
- [49] H. Zhang, Y. Liu, and H. Lei, “Localization from incomplete Euclidean distance matrix: Performance analysis for the SVD-MDS approach,” *IEEE Trans. Signal Process.*, vol. 67, no. 8, pp. 2196–2209, 2019.
- [50] J. Zhang, H.-M. Chiu, and R. Y. Zhang, “Accelerating sgd for highly ill-conditioned huge-scale online matrix completion,” *Adv. Neural Inf. Process. Syst.*, vol. 35, pp. 37 549–37 562, 2022.
- [51] R. Parhizkar, “Euclidean distance matrices: Properties, algorithms and applications,” Thesis, EPFL, 2013. [Online]. Available: https://infoscience.epfl.ch/record/196439/files/EPFL_TH5971.pdf
- [52] Z. Zhu, Q. Li, G. Tang, and M. B. Wakin, “The global optimization geometry of low-rank matrix optimization,” *IEEE Trans. Inf. Theory*, vol. 67, no. 2, pp. 1308–1331, 2021.
- [53] R. Ge, J. D. Lee, and T. Ma, “Matrix completion has no spurious local minimum,” in *Adv. Neural Inf. Process. Syst.*, vol. 29, 2016, pp. 2981–2989.
- [54] R. Ge, C. Jin, and Y. Zheng, “No spurious local minima in nonconvex low rank problems: A unified geometric analysis,” in *Proc. 34th Int. Conf. Mach. Learn.*, 2017, p. 1233–1242.
- [55] B. Vandereycken, P. A. Absil, and S. Vandewalle, “Embedded geometry of the set of symmetric positive semidefinite matrices of fixed rank,” in *Proc. IEEE/SP Workshop Statist. Signal Process.*, 2009, pp. 389–392.
- [56] F. Krahermer, S. Mendelson, and H. Rauhut, “Suprema of chaos processes and the restricted isometry property,” *Commun. Pure Appl. Math.*, vol. 67, no. 11, pp. 1877–1904, 2014.
- [57] P. Jung, F. Krahermer, and D. Stöger, “Blind demixing and deconvolution at near-optimal rate,” *IEEE Trans. Inf. Theory*, vol. 64, no. 2, pp. 704–727, 2018.
- [58] A. Ahmed, “Blind deconvolution using modulated inputs,” *IEEE Trans. Signal Process.*, vol. 68, pp. 374–387, 2020.
- [59] K. Wei, J.-F. Cai, T. F. Chan, and S. Leung, “Guarantees of Riemannian optimization for low rank matrix completion,” *Inverse Probl. Imaging*, vol. 14, no. 2, pp. 233–265, 2020.
- [60] A. S. Bandeira and R. van Handel, “Sharp nonasymptotic bounds on the norm of random matrices with independent entries,” *Ann. Probab.*, vol. 44, no. 4, pp. 2479–2506, 2016.
- [61] S. Bhojanapalli and P. Jain, “Universal matrix completion,” in *Proc. Int. Conf. Mach. Learn.*, vol. 32. PMLR, 2014, pp. 1881–1889.
- [62] R. Sun, “Matrix completion via nonconvex factorization: Algorithms and theory,” Ph.D. dissertation, University of Minnesota, 2015.
- [63] S. Lichtenberg and A. Tasissa, “Localization from structured distance matrices via low-rank matrix recovery,” *IEEE Trans. Inf. Theory*, pp. 1–1, 2024.
- [64] C. M. Smith, S. P. Lichtenberg, H. Cai, and A. Tasissa, “Riemannian optimization for euclidean distance geometry,” in *OPT 2023: Optimization for Machine Learning*, 2023.
- [65] Y. Chen, Y. Chi, J. Fan, and C. Ma, “Spectral methods for data science: A statistical perspective,” *Found. Trends Mach. Learn.*, vol. 14, no. 5, pp. 566–806, 2021.
- [66] Y. Chen, Y. Chi, J. Fan, and C. Ma, “Gradient descent with random initialization: fast global convergence for nonconvex phase retrieval,” *Math. Program.*, vol. 176, no. 1–2, p. 5–37, 2019.
- [67] J. Ma and S. Fattahi, “Convergence of gradient descent with small initialization for unregularized matrix completion,” in *Proc. Mach. Learn. Res.*, vol. 247. PMLR, 2024, pp. 3683–3742.
- [68] H. M. Berman, J. Westbrook *et al.*, “The protein data bank,” *Nucleic Acids Res.*, vol. 28, no. 1, pp. 235–42, 2000.

- [69] Y. Li, Y. Liang, and A. Risteski, "Recovery guarantee of weighted low-rank approximation via alternating minimization," in *Proc. Int. Conf. Mach. Learn.*, vol. 48. PMLR, 2016, pp. 2358–2367.
- [70] J. Chen and X. Li, "Model-free nonconvex matrix completion: Local minima analysis and applications in memory-efficient kernel pca," *J. Mach. Learn. Res.*, vol. 20, no. 142, pp. 1–39, 2019.
- [71] L. Ding and Y. Chen, "Leave-one-out approach for matrix completion: Primal and dual analysis," *IEEE Trans. Inf. Theory*, vol. 66, no. 11, pp. 7274–7301, 2020.
- [72] Y. Chen and Y. Chi, "Robust spectral compressed sensing via structured matrix completion," *IEEE Trans. Inf. Theory*, vol. 60, no. 10, pp. 6576–6601, 2014.
- [73] S. Mao and J. Chen, "Blind super-resolution of point sources via projected gradient descent," *IEEE Trans. Signal Process.*, vol. 70, pp. 4649–4664, 2022.
- [74] J. A. Tropp, "User-friendly tail bounds for sums of random matrices," *Found. Comput. Math.*, vol. 12, no. 4, pp. 389–434, 2012.
- [75] Y. Li and X. Sun, "Sensor network localization via Riemannian conjugate gradient and rank reduction: An extended version," *arXiv preprint arXiv:2403.08442*, 2024.